DOI: 10.1002/ejic.200600848

Investigation of the Thermal Decomposition of [biphen(QP*i*Pr)Pt(alk)$_2$]: An Entry to C–C Single Bond Activation?

Klaus Ruhland,*[a] Andreas Brück,[a] and Eberhardt Herdtweck[a]

Keywords: Platinum / Reaction mechanisms / C–H activation / C–C activation / Agostic interactions

The reaction of [(COD)PtCl$_2$] with biphen(QP*i*Pr)(Q′P*i*Pr) (Q, Q′ = O, CH$_2$O) yields *cis*-[{biphen(QP*i*Pr)(Q′P*i*Pr)}PtCl$_2$]. Treatment of *trans*-[PtCl$_2$(ethene)(py)] with biphen(QP*i*Pr)-(Q′P*i*Pr) (Q, Q′ = O, CH$_2$O) gives *trans*-[{biphen(QP*i*Pr)-(Q′P*i*Pr)}PtCl$_2$] for Q or Q′ ≠ O. No *trans*/*cis* isomerization can be observed for these compounds after 24 h at 105 °C in [D$_8$]toluene. In the case of Q = Q′ = O a *trans*/*cis* isomerization takes place at room temperature. X-ray structures of a molecule in the solid state were determined for the compounds *cis*/*trans*-[{biphen(QP*i*Pr)(Q′P*i*Pr)}PtCl$_2$] with Q or Q′ ≠ O. In the case of Q = O and Q′ = CH$_2$O the closer of the two bridging C atoms in the biphenyl fragment of the ligand is only 3.42 Å away from the Pt center but does not show a coupling to it in the ^{13}C NMR spectrum. Treatment of both *cis*- and *trans*-[{biphen(QP*i*Pr)(Q′P*i*Pr)}PtCl$_2$] with two equivalents of ethyl- or *n*-propylmagnesium chloride gives *cis*-[{biphen(QP*i*Pr)(Q′P*i*Pr)}PtAlk$_2$]; the X-ray structures of *cis*-[{biphen(CH$_2$OP*i*Pr)$_2$}PtEt$_2$] and *cis*-[{biphen(OP*i*Pr)$_2$}Pt-(*n*Pr)$_2$] are discussed. These complexes give the related alkene complexes as a result of β-H elimination/reductive elimination if heated to temperatures above 90 °C in [D$_8$]toluene, but none of the complexes with Q or Q′ ≠ O is stable at 95 °C. The thus-formed Pt(alkene) complex loses the alkene (ethene or propene) in a consecutive reaction. For [{biphen(CH$_2$OP*i*Pr)$_2$}PtEt$_2$], selective deuteration of the CH$_2$O group and the Pt-ethyl group proves that scrambling of deuterium into the *i*Pr methyl groups occurs (by a CH activation/insertion/β-H elimination/reductive elimination sequence) after the β-H elimination and before the loss of ethene, which at 95 °C is almost as fast as the loss of ethene. In the final alkene-free 14 e complex a fast dynamic C–H activation of the *i*Pr CH$_3$ protons by the Pt center (one H at a time) can be detected [an Isotopic Perturbation of Resonance (IPR) is found for the partially deuterated compound], which most probably prevents a further reaction of the complex (e.g. activation of the bridging C–C single bond in the biphenyl backbone or permanent coordination of PPh$_3$). H$_2$, however, is activated by the final complex, and the use of D$_2$ proves that deuterium is incorporated into the *i*Pr groups of the ligand. The reaction of [(COD)PtCl$_2$] with *o*-Br-phen(QP*i*Pr) gives *cis*-[PtCl$_2${*o*-Br-phen(QP*i*Pr)}$_2$] (X-ray structure reported), which forms *cis*-[Pt{phen(QP*i*Pr)}$_2$] upon treatment with *s*BuLi. The reaction of *trans*-[PtCl$_2$(ethene)-(py)] with *o*-I-phen(QP*i*Pr) gives *trans*-[PtCl$_2${*o*-I-phen-(QP*i*Pr)}$_2$] (X-ray structure reported), which also forms *cis*-[Pt{phen(QP*i*Pr)}$_2$] upon treatment with *s*BuLi. *cis*-[Pt{phen(CH$_2$OP*i*Pr)}$_2$] (X-ray structure reported) slowly isomerizes quantitatively at 95 °C in toluene to the *trans* complex. No product of reductive elimination can be detected up to 150 °C in mesitylene. *cis*-[Pt{phen(OP*i*Pr)}$_2$] (X-ray structure reported) forms two products − the *trans* isomer (X-ray structure reported) and most likely a dimeric *trans*-configured complex − upon heating to 95 °C. Again, no reductive elimination is observed regardless of whether the reaction is performed under argon or ethene atmosphere up to 150 °C in mesitylene. All materials were characterized by means of ^{1}H, ^{2}H, ^{13}C, ^{31}P, and ^{195}Pt NMR spectroscopy, FAB mass spectrometry, FT-IR spectroscopy, elemental analysis, and X-ray crystallography. DFT calculations (B3PW91/LANL2DZ) are also included for the most important compounds.

Introduction

We are currently searching for a way to activate and cleave the bridging C–C single bond in nonstrained biphenyl fragments, a reaction that is still without precedent, although the strained biphenylene has been successfully activated.[1] Other groups have reported their strategies, successes, and challenges in the area of C–C single bond activation.[2] Several advantages of focusing on the activation of the bridging C–C single bond in a biphenyl fragment have been discussed by us earlier,[3] and in light of this we decided to use the well-known principle of chelating assistance[4] to enhance the chance of observing the activation. Additionally, the ligand architecture is chosen in a way that in the course of the reaction a vibrational bending mode of the coordinated ligand forces the C–C single bond to approach the metal center in a promising orientation concerning an activation of it (compound **c** in Scheme 1).

Our former work[3] showed that Scheme 1 describes the behavior of [{biphen(OP*i*Pr)$_2$}PtEt$_2$] ([**1**]PtEt$_2$) well, except that the most decisive reaction (D) was not observed. Herein we report our progress with this strategy.

[a] TU München, Department Chemie, Lehrstuhl für Anorganische Chemie,
Lichtenbergstr. 4, 85748 Garching
E-mail: klaus.ruhland@ch.tum.de

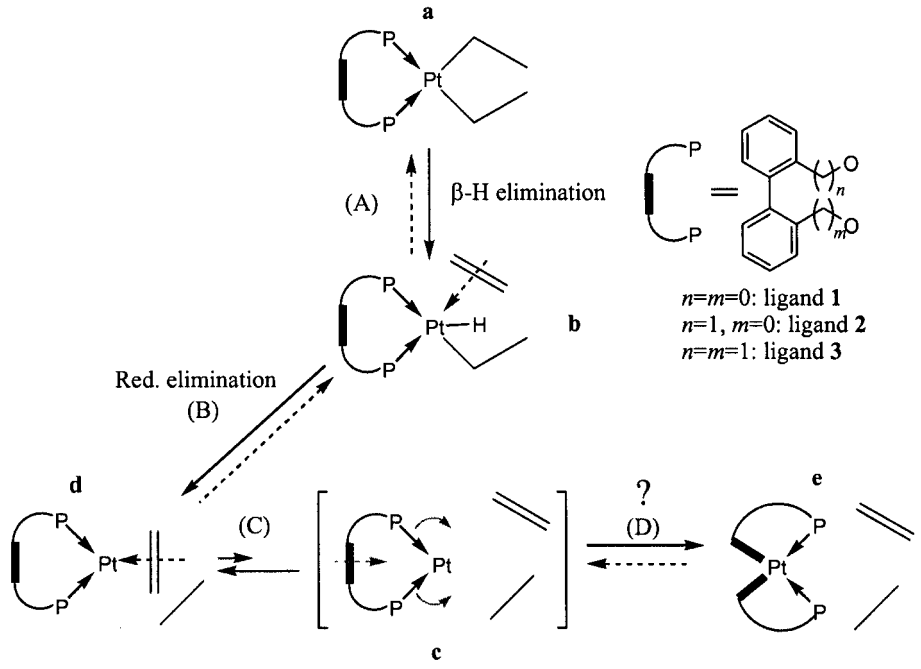

Scheme 1.

Results and Discussion

Calculations on the Reaction Path

One critical point about the strategy in Scheme 1 is that the ligand architecture used in intermediate **c** might be too strained to allow the desired movement along the reaction coordinate (bending vibration of P–Pt–P) if the biphenyl fragment and the coordinating phosphorus atoms are connected only by an oxo group. To gain more insight into this question, we calculated the energy profile of the P–Pt–P bending vibration mode with an oxo group (ligand **1**) and a CH_2O group as connector (ligand **3**). This was done with Gaussian03[5] using density functional theory (functional: B3PW91; basis set: LANL2DZ) and employing the "frozen coordinate" function implemented in the program package. Table 1 contains the calculated data and Figure 1 shows the plot of ΔG as a function of the P–Pt–P angle.

Table 1. Calculated differences between G and G_{min} of the P–Pt–P bending vibration and its dependence on the bending angle, α, for both [**1**]Pt and [**3**]Pt.

P–Pt–P α [°]	$G - G_{min}$ for [**1**]Pt [kcal mol^{-1}]	$G - G_{min}$ for [**3**]Pt [kcal mol^{-1}]
120	14.84	33.18
130	7.70	17.36
140	2.84	9.43
150	1.27	4.54
153	0	–
160	–	18.29
165	2.48	–
170	4.72	0.065
175	7.38	–
177	–	0

The following conclusions can be drawn from the calculated data:

> For ligand **1** the additional kinetic driving force concerning the C–C single bond activation is high and "downhill" at the beginning but, because of the small P–Pt–P equilibrium angle (153°), decisively "uphill" at the end of the reaction pathway. In the range $120° < \alpha < 180°$ no decisive gain in energy is predicted by the calculations because the two effects cancel each other out (energy gain of about 7 kcal mol^{-1} at most). The angle determined for [**1**]Pt-(ethene) by X-ray analysis is 120°.[3]

> For ligand **3** the additional kinetic driving force is even greater than for **1** at the beginning of the C–C single bond approach, and the equilibrium P–Pt–P angle is larger (178°). Thus, the approach of the C–C single bond to be activated is less hindered at the end of the reaction pathway. The calculations predict an energy gain of about 33 kcal mol^{-1} in the best case. Moreover, the force constant (determined using the harmonic potential approximation) in the case of ligand **3** is calculated to be 0.438 mdyn Å rad^{-2} and is thus softer than for ligand **1** (0.636 mdyn Å rad^{-2}). As a consequence, ligand **3** enhances the flexibility of the bending vibration in the area of its minimum in comparison to ligand **1**.

It must be stated at this point that the calculations give no indication of any kind of agostic interaction between parts of the ligand and the Pt center, neither through geometric proximity (the nearest H atom is more than 3 Å away from Pt) nor through the calculated wavenumbers of the vibration modes. This fact will become important below. Figure 2 shows a plot of the calculated minimum structure of [**3**]Pt.

Ligand Synthesis and Complexation

In light of the results of the calculations we synthesized the three biphen ligands **1**, **2**, and **3** (Scheme 2) to examine

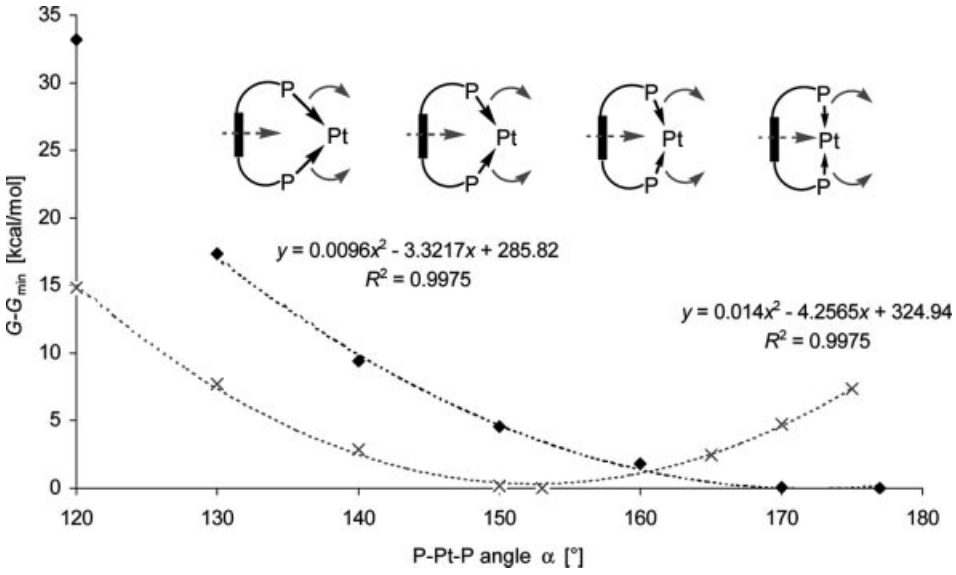

Figure 1. Potential of the P–Pt–P bending vibration for [**1**]Pt (×) and [**3**]Pt (♦) calculated using DFT theory (functional: B3PW91; basis set: LANL2DZ).

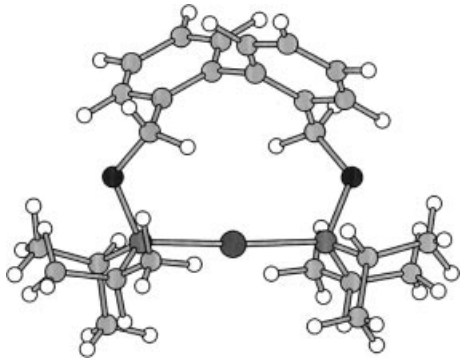

Figure 2. Plot of the calculated minimum structure of [**3**]Pt.

the influence of the ligand "arm" length on the basic strategy of Scheme 1.

The synthesis was performed analogously to our previously published procedures.[3] The precursor for **2** was synthesized from fluoren-9-one by a Baeyer–Villiger oxidation and reduction of the resulting lactone with $LiAlH_4$. We were interested in the corresponding *cis*- and *trans*-$PtCl_2$ complexes of the ligands as the *cis* compounds could serve as a precursor for the dialkyl complexes and the *trans* compounds as an experimentally available model for the transition state of the potential activation step in the thermolysis. In this context, the Cl ligands have two functions, namely they stabilize the potential transition state structure, thereby allowing us to do X-ray analysis, and because of the Cl ligands the Pt center is in the oxidation state +2, which is the oxidation state of the desired product.

In the transition state the oxidation number should, of course, be somewhere between 0 and +2. The complexes were also synthesized according to Scheme 2. The complexation reaction with ligands **2** and **3** is less clean than that with **1**, and thorough and repeated washing of the product with diethyl ether and recrystallization from dichloromethane is necessary to isolate analytically pure compounds. For **1**, which has the shortest backbone, the *trans* complex could not be isolated because it isomerizes to *cis*-[**1**]$PtCl_2$ too fast if the ligand-exchange reaction is performed at low concentrations (0.1 mmol L^{-1}) whereas a weakly soluble *trans*-configured coordination polymer is formed at higher concentrations. We propose that strain in the *trans*-[**1**]$PtCl_2$ complex is the reason for this behavior. All the other *cis*/*trans*-(ligand)$PtCl_2$ complexes show no isomerization upon heating to 105 °C in toluene for 24 h, thus demonstrating that the activation barrier for this process must be high and supporting the fact that no strain is to be expected in the transition state **c** for **2** and **3** (Scheme 1) in accordance with the results of the calculations. It should be mentioned that the synthesis of the complexes (ligand)$PtCl_2$ [*trans* (*cis*) precursor results in *trans* (*cis*) complex] is only stereoselective for $P(iPr)_2$ or PCy_2 ligand groups and not for PPh_2.

Structural and Spectroscopic Comparison of the Dichlorido Complexes

The most confident parameter to distinguish between *cis* and *trans* (diphosphane)$PtCl_2$ complexes besides an X-ray structure is the $^1J_{Pt,P}$ coupling constant, which shows values of about 4000–4200 Hz for *cis* complexes and values of about 2650 Hz for *trans* complexes.[6] This is confirmed in our case (Table 2).

The fairly large value of the *trans*-[**1**]$PtCl_2$ coupling constant (2865.5 Hz) might be due to the strain present in this compound. Additionally, the $^2J_{P,P}$ coupling constant for **2**, which has two inequivalent phosphorus atoms, shows the expected small value for the *cis* configuration (5 Hz) and a much larger value for the *trans* configuration (488.5 Hz). As can be seen from Table 2, the chemical shift in the ^{195}Pt NMR spectrum can be used as a diagnostic criterion for the complex configuration (*cis*: $\delta \approx -4100$ ppm; *trans*: $\delta \approx$

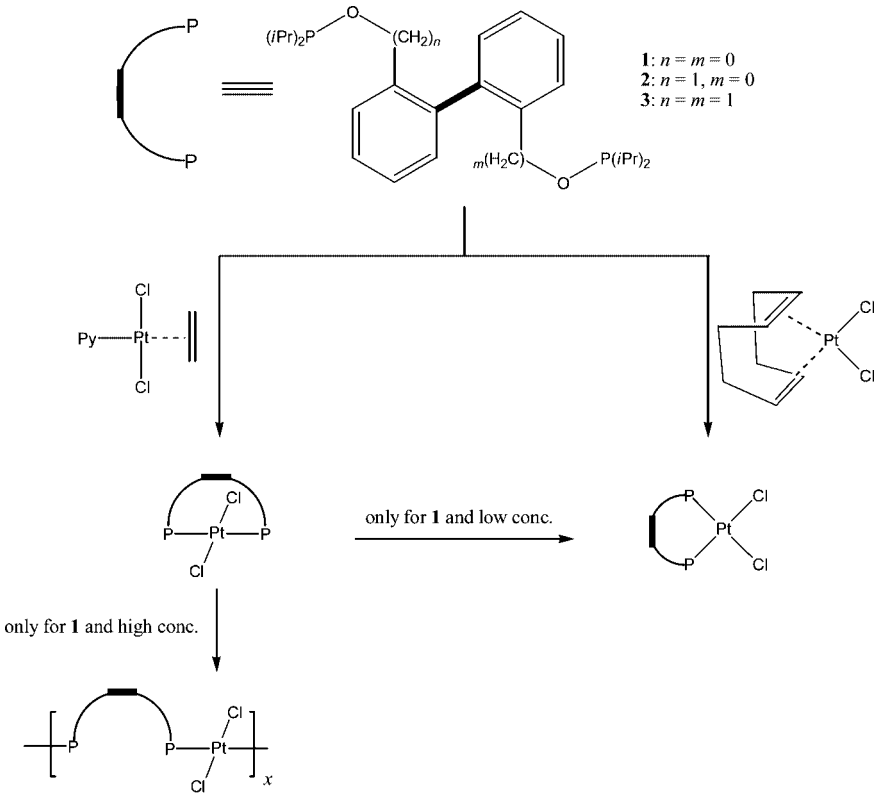

Scheme 2.

Table 2. A comparison of the NMR spectroscopic data for the compounds (ligand)$PtCl_2$.

Compound	$\delta_{^{31}P}$ [ppm]	$^1J_{Pt,P}$ [Hz]	$\delta_{^{195}Pt}$ [ppm]	$^2J_{P,P}$ [Hz]
cis-[**1**]$PtCl_2$	123.4	4147.2	–4122.8	–
trans-[**1**]$PtCl_2$	117.0	2865.5	n.d.	–
cis-[**2**]$PtCl_2$	112.5, 115.7	4099.0, 4149.6	–4116.8	5.0
trans-[**2**]$PtCl_2$	109.3, 118.8	2624.9, 2690.7	–3805.7	488.5
cis-[**3**]$PtCl_2$	115.7	4267.2	–4223.4	–
trans-[**3**]$PtCl_2$	118.4	2627.5	–3763.1	–

–3800 ppm), in contrast to the chemical shift in the ^{31}P NMR spectrum. In the case of **2** and **3**, a $^3J_{H,P}$ coupling of about 8 Hz is found for the CH_2 group in the *trans* complexes, while no H–P coupling is resolved in the *cis* complexes for the CH_2 groups. This behavior can be explained by using the structural data of a molecule in the solid state determined by X-ray diffraction. The structures of *trans*-[**2**]$PtCl_2$ and *trans*-[**3**]$PtCl_2$ are shown in Figure 3 (Table 3). Details on the the X-ray structures of *cis*-[**2**]$PtCl_2$ and *cis*-[**3**]$PtCl_2$ can be obtained from the CCDC (for more information see Exp. Sect.; relevant quality parameters of the structure determination are given in the Exp. Sect. together with all other characterization data of the compounds).

A Karplus equation for the $^3J_{P,H}$(POCH) coupling has been reported for phosphites.[7] According to this equation, the coupling constant should be small for POCH torsional angles of about 60° and have maximum values for angles of about 150–180° and 0–30°. As can be seen from Table 3, the POCH torsional angles for the *cis* complexes are about 60° and no $^3J_{P,H}$ coupling is resolved in the ^1H NMR spectra, whereas for the *trans* complexes the torsional angles are in an area for which the $^3J_{P,H}$ coupling constants are expected be about 10 Hz, in accordance with what we find in the ^1H NMR spectra. Some other structural parameters in Table 3 can be compared and discussed as follows:

> Due to a canceling *trans* influence in the *trans* complexes, the Pt–P bond is significantly longer than those in the *cis* complexes (the Pt–Cl bond behaves in the opposite manner as it is longer in the *cis* complexes).

> In spite of the fact that the bridging C–C single bond of the biphenyl fragment in *trans*-[**2**]$PtCl_2$ is only about 3.42 Å

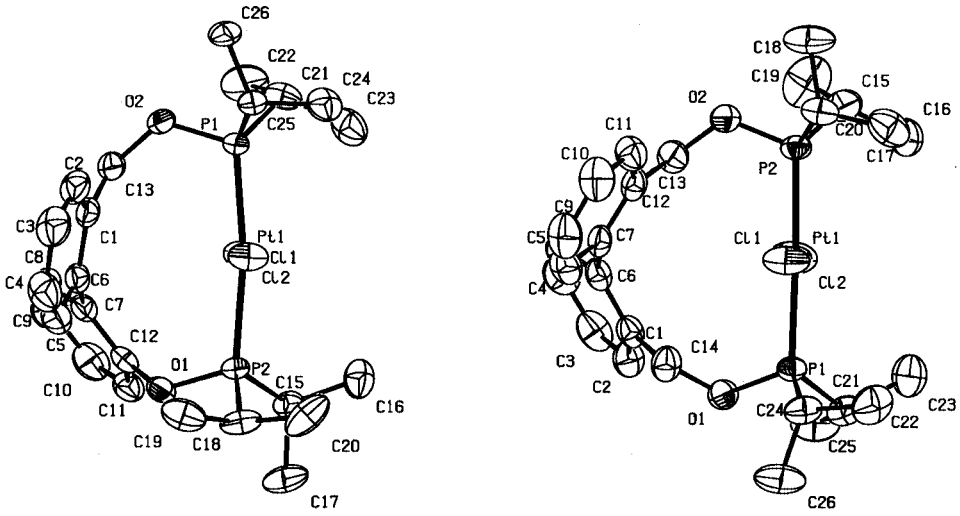

Figure 3. ORTEP style plot of the compounds *trans*-[**2**]$PtCl_2$ (left) and *trans*-[**3**]$PtCl_2$ (right) in the solid. Thermal ellipsoids are drawn at the 50% probability level. Hydrogen atoms have been omitted for clarity.

Table 3. A comparison of the geometric data for the compounds (ligand)$PtCl_2$ determined by X-ray analysis.

	cis-[**1**]$PtCl_2$[3]	*cis*-[**2**]$PtCl_2$	*cis*-[**3**]$PtCl_2$	*trans*-[**2**]$PtCl_2$		*trans*-[**3**]$PtCl_2$
Pt–P1 [Å]	2.2321(12)	2.2421(13)	2.238(3)	2.3103(15)	2.3167(16)	2.3169(12)
Pt–P2 [Å]	2.2291(11)	2.2527(15)	2.236(3)	2.3076(15)	2.3110(15)	2.3292(13)
Pt–Cl1 [Å]	2.3671(12)	2.3579(13)	2.379(3)	2.2993(15)	2.3135(13)	2.3017(12)
Pt–Cl2 [Å]	2.3534(12)	2.3591(13)	2.374(3)	2.3148(15)	2.2992(15)	2.3083(13)
C6–C7 (bridge) [Å]	1.483(7)	1.486(8)	1.492(15)	1.482(9)	1.494(9)	1.492(7)
Pt···C6 [Å]	4.391(4)	4.865(5)	6.226(14)	3.419(7)	3.457(7)	4.132(5)
Pt···C7 [Å]	4.896(4)	5.433(6)	6.256(13)	3.657(6)	3.720(6)	4.255(5)
P–Pt–P [°]	95.52(4)	95.90(5)	96.61(11)	171.50(6)	170.29(6)	177.91(4)
Cl–Pt–Cl [°]	89.12(4)	85.60(4)	85.44(10)	178.43(6)	177.77(6)	173.49(6)
Torsional angle HC13/14OP [°]	–	Hα 59 Hβ –61	Hα –67 Hβ 52	Hα –44 Hβ –162	Hα 50 Hβ 167	Hα –25 Hβ –5 Hα′ –143 Hβ′ –23

apart from the metal center, no $J_{Pt,C}$ coupling can be detected in the ^{13}C NMR spectrum and, thus, no evidence for an interaction between these two centers can be found.

> In accordance with this finding no significant elongation of the bridging C–C single bond in the biphenyl fragment is found in *trans*-[**2**]$PtCl_2$ or *trans*-[**3**]$PtCl_2$.

> The P–Pt–P bond angle of about 178° in *trans*-[**3**]$PtCl_2$ is in good agreement with the calculated data for [**3**]Pt, thereby showing that the theoretical results are fairly confident and a structural comparison of the two compounds is justified.

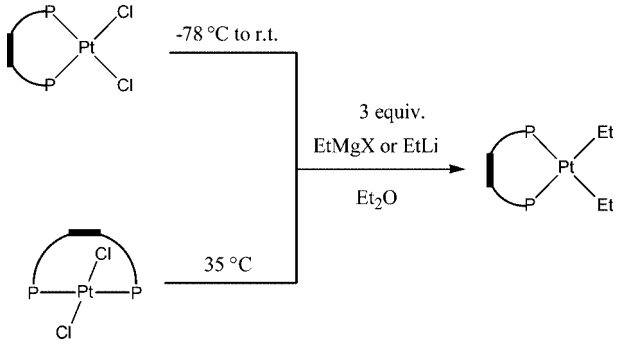

Scheme 3.

Alkylation of the Dichlorido Complexes

Treatment of *cis*-[**2**]$PtCl_2$ and *cis*-[**3**]$PtCl_2$ with ethylmagnesium chloride at low temperatures in diethyl ether yielded the corresponding *cis*-(ligand)$PtEt_2$ complexes, which are the starting compounds **a** in Scheme 1. The analogous complexes *trans*-[**2**]$PtCl_2$ and *trans*-[**3**]$PtCl_2$ showed no reaction at low temperature, even with EtLi. Alkylation was possible, though, in refluxing diethyl ether with both ethylmagnesium chloride and EtLi to give *cis*-(ligand)$PtEt_2$ rather than the *trans* complexes (Scheme 3).

We propose the following mechanism to explain this behavior (Scheme 4). The slower reaction of the *trans*-(ligand)$PtCl_2$ complexes is explained by transition state **T1**, which is sterically crowded and is therefore formed slowly in comparison to transition state **C1**. It is proposed that a fast Berry pseudorotation transforms **T1** into the sterically and electronically preferred **C1**. It will be shown later in this publication that the chelating character of the phosphinite ligand is not the decisive factor in this mechanism. We propose that the combination of an alkyl substituent, a halide,

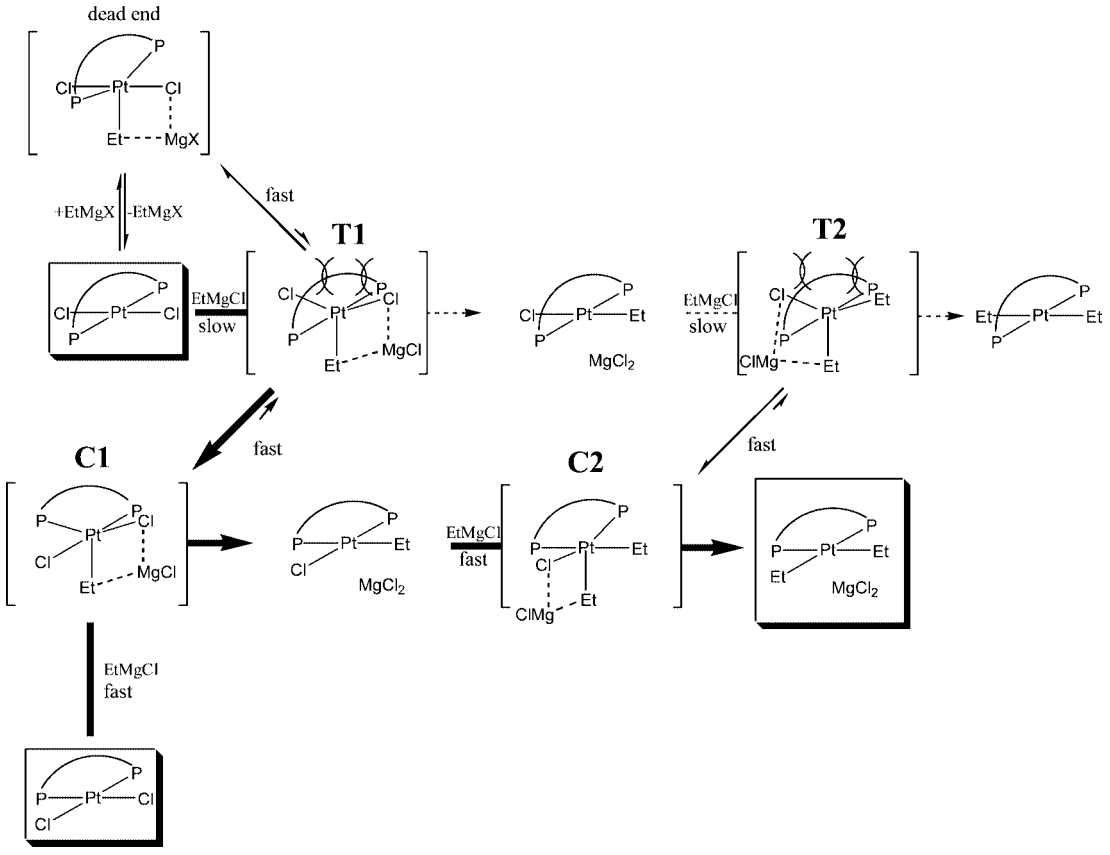

Scheme 4.

and a phosphinite in an equatorial position in **C1** and **C2** is electronically favored because of a synergistic cooperation of a strong σ-donor (alkyl) and a strong π-acceptor (phosphinite), both of which weaken the Pt–Cl bond and thus lower the activation energy. Even if the *trans*-(ligand)PtEtCl complex is partly formed, when generating **T2** there is a second chance for the reaction to switch into the *cis* pathway (**C2**), again by a Berry pseudorotation. This is the reason why *cis*-(ligand)PtEt$_2$ is formed exclusively from the *trans*-(ligand)PtCl$_2$ complex. The mechanism proposed in Scheme 4 is supported by the finding that the use of one equivalent of ethylmagnesium chloride results in the formation of a mixture of *cis*-(ligand)PtCl$_2$, *cis*-(ligand)PtEtCl, and *cis*-(ligand)PtEt$_2$ (3:2:1) if *cis*-(ligand)PtCl$_2$ is the starting material. In the case of *trans*-(ligand)PtCl$_2$, though, the product is a mixture of unchanged *trans*-(ligand)PtCl$_2$ and *cis*-(ligand)PtEt$_2$ only; no monoethyl complex is formed.

Relevant quality parameters of the crystal structure determinations of compounds *cis*-[**1**]Pt(*n*Pr)$_2$ and *cis*-[**3**]PtEt$_2$ are given in the Exp. Sect. together with all other characterization data of the compounds. Some key data are summarized in Table 4. The X-ray structures of *cis*-[**1**]PtEt$_2$ and *cis*-[**1′**]PtEt$_2$ (**1′** = **1**, but with phenyl substituents at the phosphorus atom instead of *i*Pr) have been published by us previously.[3]

Table 4. A comparison of the geometric data for two (ligand)-Pt(alk)$_2$ compounds, as determined by X-ray analysis.

	[**1**]Pt(*n*Pr)$_2$	[**3**]PtEt$_2$
Pt–P [Å]	2.2784(6)	2.2657(14)
Pt–C [Å]	2.152(3)	2.124(4)
C_a–C_b(bridge) [Å]	1.477(4)	1.480(7)
Pt···C_a [Å]	4.377(3)	6.316(5)
P–Pt–P [°]	111.87(2)	96.15(4)
alk–Pt–alk [°]	86.56(10)	82.72(17)

The main difference in the structures of *cis*-[**1**]Pt(alk)$_2$ and *cis*-[**3**]PtEt$_2$ is that a decisive extension of the P–Pt–P angle in **1** to values larger than 90° is observed; this is much less pronounced in the case of **3**.

Thermolysis Behavior

The thermolysis of *cis*-[**1**]PtEt$_2$ in the temperature range 60–110 °C has been reported by us in detail.[3] The major result concerning our strategy in Scheme 1 is that [**1**]Pt(ethene) is formed by β-H elimination and reductive elimination of ethane without the permanent loss of ethene. This means that the ethene is firmly bound. Its dissociation could be proven only indirectly by trapping reactions and kinetic analysis of the Pt(ethene)/(free ethene) exchange (Scheme 5).

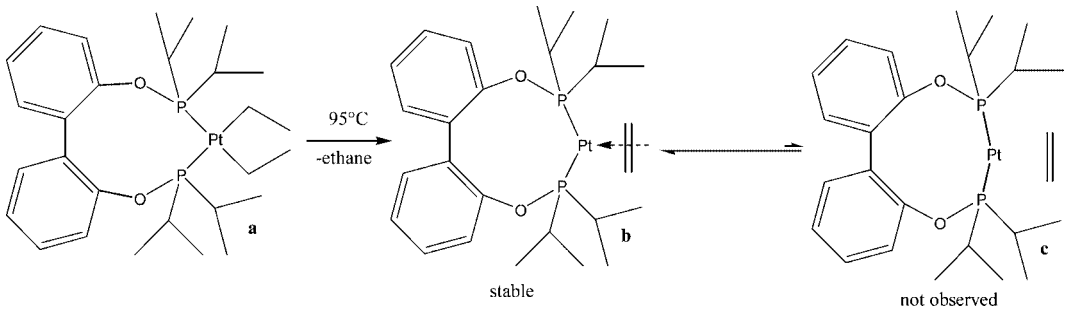

Scheme 5.

To labilize the alkene sterically we examined *cis*-[**1**]-Pt(*n*Pr)$_2$ in the thermolysis reaction. *cis*-[**1**]Pt(*n*Pr)$_2$ forms [**1**]Pt(propene) at 80 °C, which is not stable and decomposes in a not well defined manner while losing propene, further supporting the proposal that the ligand backbone architecture in **1** is too rigid to approach the metal center. The [**1**]-Pt thus formed can be trapped cleanly by treatment with H_2SiEt_2 to give the Si-H oxidative addition product. For *cis*-[**2**]PtEt$_2$ and *cis*-[**3**]PtEt$_2$ the (ligand)Pt(ethene) complex is clearly formed in the course of the thermolysis, but it is not stable at 95 °C and further reacts cleanly and completely to a final product with the formation of free ethene (which was not observed in the case of [**1**]PtEt$_2$) and ethane (δ = 5.3 and 0.8 ppm, respectively in the ^{1}H NMR spectrum; ethene/ethane ratio of 1:1. This quantification is better performed by ^{2}H NMR spectroscopy and [**3**]Pt(D$_5$-Et)$_2$ as starting material because in this case no peak overlaps with the *i*Pr groups are observed in the region around δ = 0.8 ppm). The compound thus formed could not be isolated but its assignment as a (ligand)Pt(ethene) complex due to its chemical shift in the ^{31}P and ^{195}Pt NMR spectra as well as the $^1J_{P,Pt}$ coupling constants (Table 5) is unequivocal. The small $^2J_{P,P}$ coupling constant in [**2**]Pt(ethene) suggests that the P–Pt–P bond angle is not much larger than 90° and it is similar to that found for [**1**]Pt(propene).

Table 5. NMR spectroscopic data for the compounds (ligand)Pt(alkene) and (ligand)Pt.

Compound	$\delta_{^{31}P}$ [ppm]	$\delta_{^{195}Pt}$ [ppm]	$^1J_{P,Pt}$ [Hz]	$^2J_{P,P}$ [Hz]
[**1**]Pt(ethene)[3]	186.3	–5105.4	3999.7	–
[**1**]Pt(propene)	185.7, 185.5	n.d.	4181.5, 3658.9	16.2
[**2**]Pt(ethene)	172.1, 172.4	–5002.7	3881.1, 3959.4	11.8
[**3**]Pt(ethene)	177.5	–5077.9	4133.7	–
[**2**]Pt	144.8, 156.3	–4770.7	3178.8, 3262.0	486.6
[**3**]Pt	160.1	–4894.8	3158.8	–

Figure 4 shows the kinetic development of the thermolysis of [**3**]PtEt$_2$ followed by ^{31}P NMR spectroscopy at 95 °C. The pseudo triplet at about δ = 145 ppm belongs to the starting material, the [**3**]Pt(ethene) intermediate shows up at about δ = 177 ppm, and the final product at 95 °C appears at about δ = 160 ppm quantitatively. The question now arises as to what is the nature of this final product.

In order to answer this question we examined the final product by means of FAB-MS and FT-IR, ^{1}H, ^{13}C, ^{31}P, and ^{195}Pt NMR spectroscopy. The FAB mass spectrum for [**3**]-PtEt$_2$ shows the mass peak at *m*/*z* 641.3 (M minus ethene and ethane with correct isotopic pattern). The mass peak for the final product [**3**]Pt shows up at *m*/*z* 642.3 and the

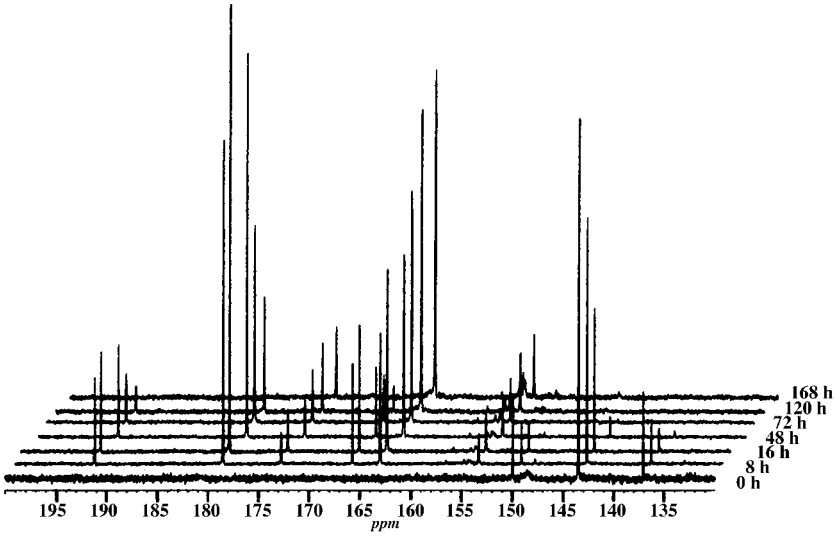

Figure 4. ^{31}P NMR spectra recorded during the thermolysis of [**3**]PtEt$_2$ at 95 °C in [D$_8$]toluene.

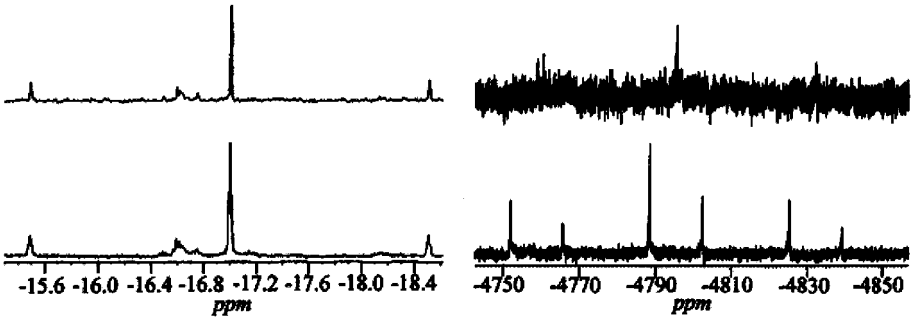

Figure 5. Portions of the ^{1}H (left) and ^{195}Pt (right) NMR spectra showing the Pt–H signals. Top: ^{1}H{^{31}P} and ^{195}Pt{^{1}H}.

isotopic pattern is correctly reproduced assuming the loss of both ethane and ethene during the course of the thermolysis (98% M + 1 and 2% M with M = $C_{26}H_{40}O_2P_2Pt$ = [**3**]Pt). That the final product contains only the ligand **3** and Pt is also supported by the fact that performing the thermolysis with [**3**]Pt(*n*Pr)$_2$ results in the same final product as is found with [**3**]PtEt$_2$, according to ^{1}H, ^{13}C, ^{31}P, and ^{195}Pt NMR spectroscopy as well as FT-IR spectroscopy and FAB-MS. In the case of [**3**]Pt(*n*Pr)$_2$ the intermediate [**3**]Pt(propene) was not observed and free propene instead of ethene was found (^{1}H NMR spectroscopy). However, ^{1}H NMR spectroscopy shows a peculiarity concerning the final product [**3**]Pt: a triplet of pseudo triplets at δ = –17 ppm can be found which integrates to about 0.7 H atoms relative to the CH_2–O protons and the phenyl C–H protons as internal standard (Figure 5). In the FT-IR spectrum an unusual peak of low intensity appears at $\tilde{\nu}$ = 1945 cm^{-1} (Figure 9).

The pseudo triplet (1208.5 Hz splitting) is unequivocally due to a $^1J_{Pt,H}$ coupling, while the triplet (4.9 Hz splitting) was proven to be a $^2J_{P,H}$ coupling from the ^{1}H{^{31}P} NMR spectrum, in which this coupling disappears (Figure 5, top left). A doublet (1208.5 Hz) of triplets (3160 Hz) in the ^{195}Pt NMR spectrum can be found using the default ^{195}Pt{^{1}H} acquisition program with the ^{1}H decoupler center at δ = 5 ppm (Figure 5, bottom right). If the decoupler center is changed to δ = –17 ppm the doublet splitting in the ^{195}Pt NMR spectrum vanishes (Figure 5, top right). From this finding we conclude that one and only one H atom (at a time) is in strong electronic interaction with the Pt center. This H atom must be placed in such a manner that the complex (at least in average) has at least C_2 symmetry since only one signal (pseudo triplet) is found for the P atoms (Figure 4). The small $^2J_{P,H}$ coupling constant of about 5 Hz mentioned before suggests that the angle between the P atoms and the H atom is about 90°. The $^1J_{Pt,P}$ coupling constant of 3160 Hz is in accordance with the *trans* P–Pt–P orientation that would be expected for [**3**]Pt in light of the above calculations. Furthermore, the $^3J_{P,H}$ coupling constants of 7 and 12 Hz in the $POCH_2$ fragment indicate a *trans* configuration. This is further supported by the fact that a $^2J_{P,P}$ coupling constant of 485 Hz is found for [**2**]Pt, which shows similar peculiarities in the ^{1}H and ^{195}Pt NMR spectra but is not stable even at room temperature and decomposes into as-yet unknown products within a few hours. In the ^{13}C{^{1}H} NMR spectrum of [**3**]Pt a coupling to the Pt center is observed for the CH_2O carbons (83.7 Hz) and one CH_3 group (22.1 Hz), which is slightly separated from the other methyl groups to higher fields by about 1 ppm. The signals of the other CH_3 groups overlap but clearly show a structure different from simple singlets. For the P-CH carbons only a coupling to phosphorus is found. No coupling of Pt to any of the aromatic carbons could be detected.

Deuteration Experiments

We wanted to get more insight into the peculiarity mentioned above. Thus, we first selectively deuterated the CH_2O groups to examine whether they are the origin of the peak at δ = –17 ppm in the ^{1}H NMR spectrum. This deuteration was achieved by reduction of biphenic acid with $LiAlD_4$. The [D_4-**3**]Pt formed in the course of thermolysis shows, analogously to [**3**]Pt, the expected peak at M + 1 (*m*/*z* 646.1) with the correct isotopic pattern in the FAB mass spectrum. In the ^{2}H NMR spectrum the CD_2O protons show up as two broad, unresolved peaks at the same chemical shift as was found for the CH_2O groups of [**3**]Pt in the ^{1}H NMR spectrum, while no peak is observed at δ = –17 ppm. In the ^{1}H NMR spectrum the multiplets for the CH_2O groups are missing and the peak at δ = –17 ppm is present with the same intensity as was observed for [**3**]Pt. In the ^{31}P and ^{195}Pt NMR spectra no difference with respect to the unlabeled complex can be seen. From these findings we conclude that the CH_2O protons are not responsible for the observed interaction with the platinum center. We next selectively deuterated the ethyl groups in [**3**]-$PtEt_2$ by using commercial CD_3CD_2Br in a Grignard reaction. The thermolysis of [**3**]Pt(D_5-Et)$_2$ occurs slower than that of [**3**]PtEt$_2$, thus indicating a normal kinetic isotope effect for the reaction, which we did not quantify. The product of the thermolysis shows a peak pattern for the mass peak in the FAB mass spectrum that is best described as a superposition of 65% [**3**]Pt and 35% of [D_1-**3**]Pt, thus giving a first hint that the complete reaction is more complicated than we had anticipated initially. In the ^{1}H NMR spectrum the most obvious difference is that besides the

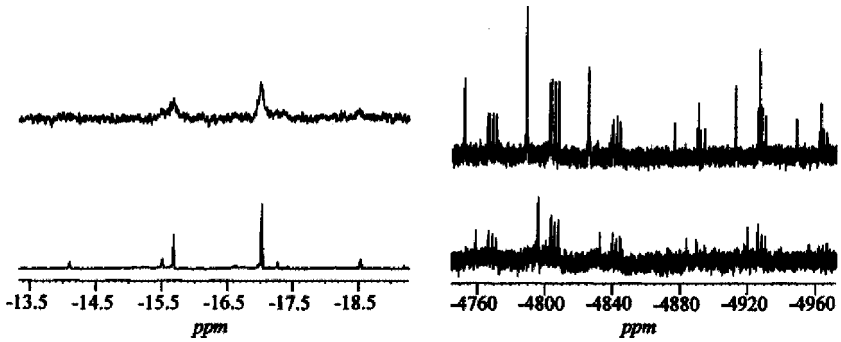

Figure 6. Excerpt of the ^{1}H (bottom left), ^{2}H (top left), ^{195}Pt (top right), and $^{195}Pt\{^{1}H\}$ (bottom right) NMR spectra showing the Pt–H(D) signals.

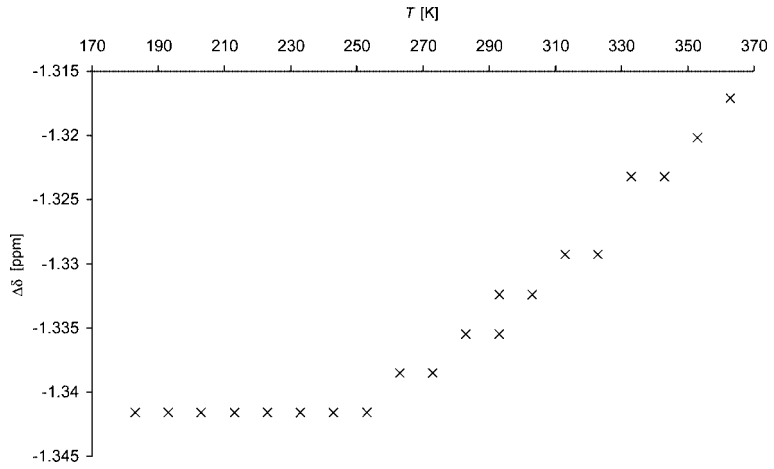

Figure 7. Temperature dependence of the chemical-shift difference, $\Delta\delta$, in the ^{1}H NMR spectrum between the two peaks at about δ = –15.5 and –17 ppm.

pseudo triplet of triplets at δ = –17 ppm an additional peak with the same multiplicity shows up (ratio 2:1) at about δ = –15.5 ppm ($^{1}J_{Pt,H}$ = 1266.1, $^{2}J_{P,H}$ = 3.7 Hz), which together integrate to 0.7 protons (Figure 6).

Since we expected that the origin of the second peak should be an isotopic perturbation of resonance (IPR[9]) we performed variable-temperature measurements in the temperature range –90 °C to +90 °C (Figure 7).

As can be seen from Figure 7, a small but significant temperature-dependent change in $\Delta\delta$ between the two peaks at about δ = –15.5 and –17 ppm is observed, which supports the existence of an IPR. In the temperature range in which $\Delta\delta$ remains constant (below 253 K), the signals in the ^{2}H NMR spectrum broaden significantly and almost disappear with decreasing temperature. We conclude from this that ^{1}H and not ^{2}H atoms are predominantly found at low temperatures in the "hydrido" position (responsible for the peaks at negative ppm), which is in accordance with theory.

In the ^{2}H NMR spectrum peaks for ethene and ethane appear along with the signals at δ = –15.5 and –17 ppm, and a peak group in the area of 1 ppm also shows up where the CH_3 groups are found in the ^{1}H NMR spectrum (Figure 8).

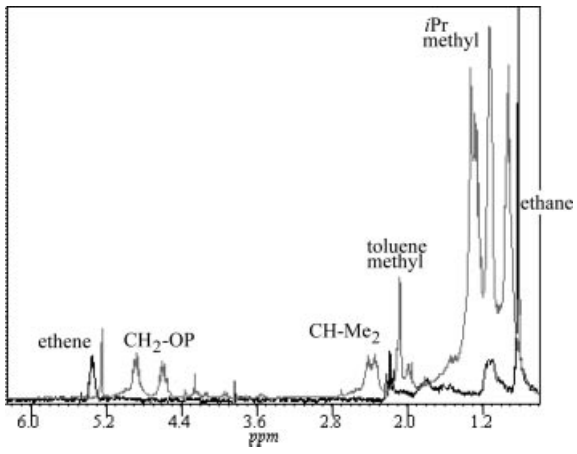

Figure 8. ^{1}H NMR spectrum (grey) of [**3**]Pt in [D_8]toluene and the ^{2}H NMR spectrum of [D_m-**3**]Pt (m: number of incorporated deuterium atoms into the ligand in the course of the thermolysis) in non-deuterated toluene (black) in the region between 0.7 and 6 ppm.

The FT-IR spectrum shows two new peaks (Figure 9), one at 2224 cm^{-1}, which in accordance with the ^{2}H NMR findings we assign to aliphatic C–D stretching vibrations,

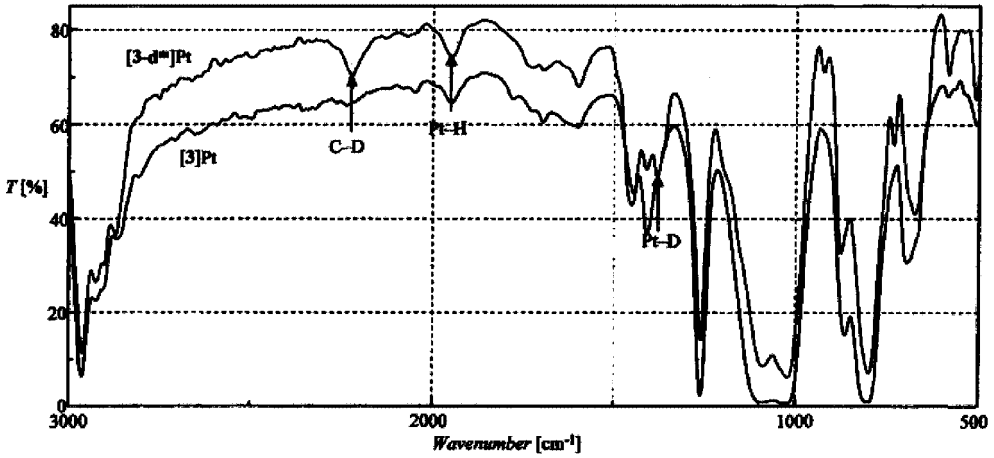

Figure 9. FT-IR spectra for [D$_m$-**3**]Pt and [**3**]Pt.

and one at 1383 cm^{-1}, which we assign to a Pt–D stretching vibration corresponding to the peak at 1945 cm^{-1}.

The ^{13}C NMR spectrum, in accordance with the ^{1}H NMR results, contains two very close sets of signals for each carbon ($\Delta\delta \approx -0.15$ ppm, ratio 2:1), with the more intense set being identical to the unlabeled case. A $J_{C,D}$ coupling could not be unequivocally detected for any of the carbons, although the methyl signals overlap and, thus, are not clearly resolved. A similar kind of experimental finding in the ^{13}C NMR spectrum (desymmetrization by partial deuteration) has been used (among several other cases) to prove that the keto–enol tautomerization equilibrium in acetylacetone contains two energetic minima with asymmetric hydrogen bonds between the oxygens, the symmetric connectivity being a transition state rather than an intermediate.[9f] This supports our findings and conclusions concerning the ^{1}H and ^{2}H NMR spectra.

The ^{31}P NMR spectrum shows two very close groups of signals (δ = 163.6 and 164.1 ppm, ratio 1:2; Figure 10), which correspond to the two signals at negative ppm in the ^{1}H NMR spectrum, thus demonstrating that several different compounds are present at the end of the thermolysis that are very similar to each other (Figure 10). ^{195}Pt NMR spectroscopy, which, in general, provides only limited information, is very powerful in this specific case. In accordance with the ^{1}H and ^{2}H NMR spectra four different compounds are detected at very similar chemical shifts, two of them have an almost identical chemical shift and can only be distinguished by the coupling pattern, which provides a $^{1}J_{Pt,H}$ coupling (doublet splitting, $^{1}J_{Pt,H}$ identical to that in the ^{1}H NMR spectrum) in one case and a $^{1}J_{Pt,D}$ coupling (triplet splitting with about 1/7th of the magnitude of $^{1}J_{Pt,H}$) in the second case (Figure 6). This is further support for the desymmetrization by partial deuteration found by ^{1}H, ^{2}H, ^{13}C, and ^{31}P NMR spectroscopy.

A more detailed examination of the thermolysis was performed by ^{2}H and ^{31}P NMR spectroscopy (Figure 10).

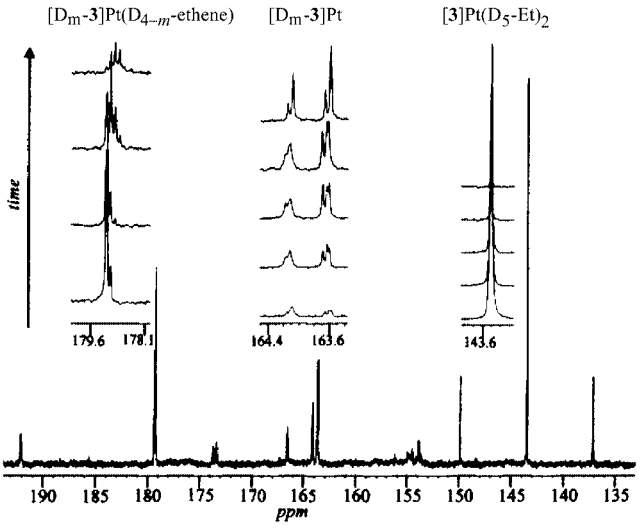

Figure 10. Time-dependent ^{31}P NMR spectra for the thermolysis of [**3**]Pt(D$_5$-Et)$_2$ showing the scrambling of deuterium into the ligand during the reaction.

As can be seen from Figure 10, the signal of the intermediate [**3**]Pt(D$_4$-ethene) splits with time due to a scrambling of deuterium into the *i*Pr groups of the ligand, as proven by ^{2}H NMR spectroscopy (Figure 8). This scrambling also leads to a peak splitting in the final product [**3**]Pt. The starting material does not show any splitting. Isolated [D$_m$-**3**]Pt does not change its peak pattern upon further heating. If the same experiment is performed with [**3**]Pt(D$_5$-Et)$_2$ under an atmosphere of unlabeled ethene the scrambling in both [D$_m$-**3**]Pt(D$_{4-m}$-ethene) and [D$_m$-**3**]Pt is still observed, thus proving that the scrambling process is faster than the loss or exchange of ethene. If the thermolysis of [**3**]PtEt$_2$ is performed under an atmosphere of H$_2$, no ethene can be detected. Instead, *trans*-PtH$_2$ shows up in small amounts in

the ^{1}H NMR spectrum (δ = –2.45 ppm, $^2J_{P,H}$ = 21.2, $^1J_{Pt,H}$ = 799 Hz; cf. *cis*-[**1**]PtH$_2$: δ = –3.43 ppm, $^2J_{P,Hcis}$ = 31.8, $^1J_{Pt,H}$ = 1029.5 Hz[3]). [**3**]Pt is still the final product. If D_2 is used instead of H_2, the final product is [D_m-**3**]Pt, which shows the same splitting in the ^{1}H and ^{31}P NMR spectra due to deuterium scrambling into the ligand as is found with [**3**]Pt(D_5-Et)$_2$ as starting material (although in different ratios), whereas this time no scrambling is found in the intermediate [**3**]Pt(ethene) (or in [**3**]PtEt$_2$). Additionally, when using D_2 a small peak for *trans*-[**3**]PtH$_2$ and an even smaller peak for *trans*-[**3**]PtHD (δ = –2.27 ppm, $^2J_{P,H}$ = 21.2, $^2J_{HD}$ ≈ 1 Hz) can be detected in the ^{1}H NMR spectrum after some time. If the final product [**3**]Pt (without labelling) is heated under an atmosphere of D_2, incorporation of deuterium can again be detected, but this occurs more slowly than during the thermolysis starting from [**3**]PtEt$_2$.

Finally, if [**3**]Pt is treated with PPh_3 in excess in [D_8]toluene the signal for PPh_3 in the ^{31}P NMR spectrum is broadened and appears almost at the same position as free PPh_3. This broadening cannot be frozen out even at –100 °C. For [**3**]Pt, the only peaks that broaden are those in the ^{195}Pt NMR spectrum. We can therefore conclude from these findings that there is contact between the PPh_3 and the Pt center, but the interaction is only weak. [**1**]Pt(ethene), in contrast, quantitatively coordinates PPh_3 at room temperature (triplet at δ = 41 ppm with $^1J_{Pt,P(Ph)}$ = 3969.3, $^2J_{P,P}$ = 192.2 Hz and doublet at δ = 199.2 ppm with $^1J_{Pt,P(iPr)}$ = 4910.6, $^2J_{P,P}$ = 192.2 Hz).

Explanation of the Behavior

Agostic interactions between the ligands' H atoms and the metal center are not uncommon, especially in 14-electron complexes.[8] There is precedence for this (at least) with group 8, group 9, and group 10 metals, for which agostic interactions to C–H bonds in P-Ph, P-*t*Bu, and P-Cy ligand fragments have been found. However, in all these cases the P-*i*Pr fragment turned out to be an exception and showed no such interaction, especially not in {P(*i*Pr)$_3$}$_2$Pt.[8a] However, in our case there is strong experimental evidence for an interaction between the *i*Pr methyl groups and the Pt^0 center.

We ascribe the second peak at δ = –15.5 ppm in the ^{1}H NMR spectrum of the final product when performing the thermolysis with [**3**]Pt(D_5-Et)$_2$ to a dynamic equilibrium concerning a C–H activation of the *i*Pr methyl groups by the Pt^0 center as shown in Scheme 6.

This peak at δ = –15.5 ppm proves that the symmetric structure with two agostic interactions shown in the center of Scheme 6 can only be a transition state. The ground states must therefore be asymmetric (IPR). This is supported by the ^{195}Pt NMR spectrum, which shows only one Pt···H interaction at a time, and by the second set of signals in the ^{13}C NMR spectrum upon partial deuteration, which is an additional indicator for an IPR.

We propose the behavior in Scheme 7 to explain the experimental results. [**3**]PtEt$_2$ irreversibly loses ethane by a β-H elimination/reductive elimination if heated to 95 °C. The [**3**]Pt(ethene) complex (**2**) intramolecularly C–H activates the *i*Pr methyl groups of the ligand and the coordinated ethene inserts reversibly into the Pt–H bond via compound **4b**. Indirect evidence for the existence of **4b** is given by the incorporation of deuterium into the *i*Pr methyl groups if the thermolysis is performed with [**3**]Pt(D_5-Et)$_2$ (Figure 8 and Figure 10). Compounds **2** and **4a** in Scheme 7 lose ethene reversibly to form ethene-free [**3**]Pt, which must be thermodynamically more stable than **2** and **4** because if [D_m-**3**]Pt is heated to 95 °C under an atmosphere of unlabeled ethene instead of argon, **2** cannot be detected and the degree of labelling in [D_m-**3**]Pt slowly decreases (over days). The loss of ethene is compensated in [**3**]Pt by the dynamic interaction of two *i*Pr methyl groups of the ligand with the Pt center (one at a time, because an IPR was found).

That the interaction between the Pt center and the *i*Pr groups of the ligand (**3** in Scheme 7) must be strong is further supported by the finding that pyridine and PPh_3 are not permanently coordinated even at 100 °C in toluene.

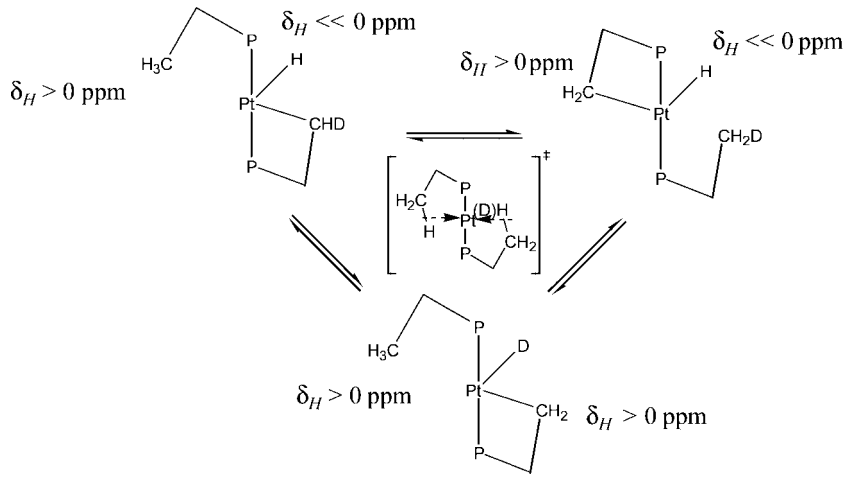

Scheme 6.

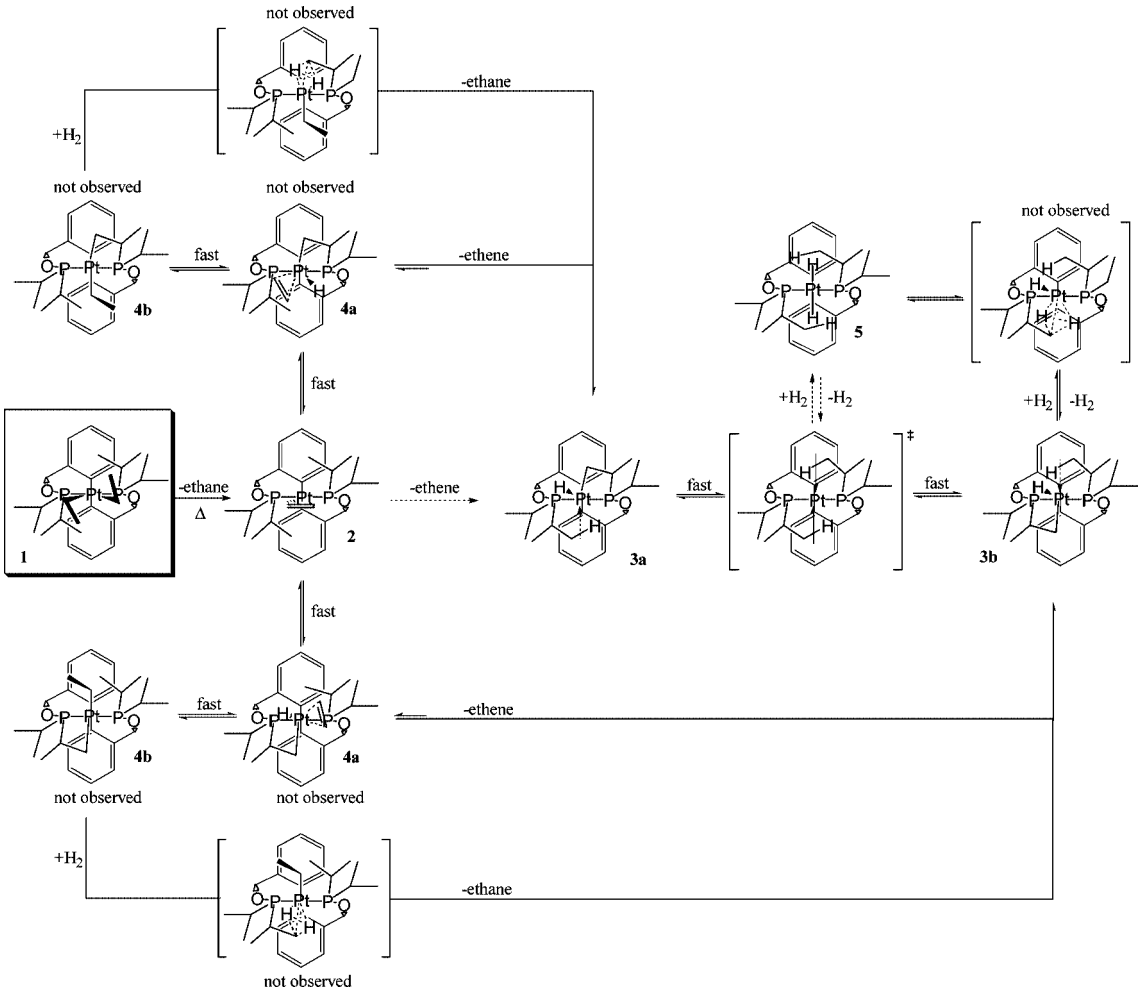

Scheme 7.

Since no incorporation of deuterium into **2** can be detected when doing the thermolysis under an atmosphere of D_2, neither **2** nor **4a** can be attacked by D_2 (nor can **1**). The finding that the incorporation of deuterium into **3** is faster during the thermolysis under D_2 atmosphere than when heating **3** under D_2 at the same temperature is further indirect evidence for the existence of **4b**. The reaction pathway via **4b** also explains why no ethene can be detected during the thermolysis under an atmosphere of H_2.

All these findings can be explained by the mechanism proposed in Scheme 7. Unfortunately, we have not yet been able to grow single crystals of [**3**]Pt suitable for X-ray analysis. The most similar kind of interaction to the one described here, that we are aware of, was reported by Crabtree et al. with an Ir^{III} complex,[8l] where two *ortho*-phenyl C–H bonds are found to dynamically oxidatively add to the Ir center.

Approach from the Product Side

In a previous publication we reported on the problems to synthesize the expected products of the anticipated activation process via orthometalated precursors because of a rearrangement taking place.[3] We have since overcome these problems by first coordinating the phosphinites to the platinum center and then performing the orthometalation followed by salt metathesis (the last two steps in a one-pot reaction) using *s*BuLi in toluene.

The complexes *trans*-(ligand)^{X}PtCl$_2$ can be synthesized from the *ortho*-iodophosphinite as precursor (relevant quality parameters of the crystal structure determination are given in the Exp. Sect. together with all other characterization data of the compounds). For the *cis* isomers the *ortho*-iodophosphinite precursor cannot be used, presumably because of an intramolecular oxidative addition. Only an unidentified mixture of products can be isolated if (COD)PtCl$_2$ is treated with *ortho*-iodophosphinite. Switching to the less reactive *ortho*-bromophosphinite solves this problem and leads to the desired product in good yield (relevant quality parameters of the crystal structure determination are given in the Exp. Sect. together with all other characterization data of the compounds).

The ^{31}P NMR signal of *cis*-[**1***]^{Br}PtCl$_2$ broadens with decreasing temperature, thus indicating a dynamic process with an approximate activation enthalpy of about 6 kcal mol^{-1} (line shape analysis), which we assign to a re-

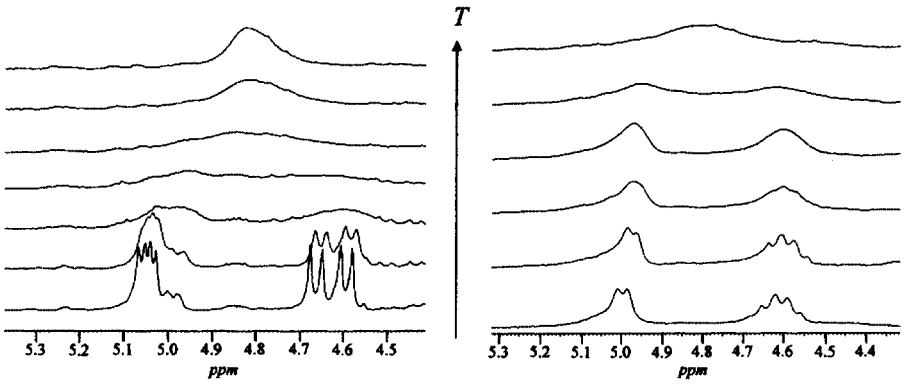

Figure 11. Results of the variable-temperature ^{1}H NMR measurements for the OCH_2 protons in *cis*-[**3***]Pt (left) and *trans*-[**3***]Pt (right) between –90 and 100 °C.

stricted rotation about the P–Pt axis. This is supported by the crystal structure determination. Similar to the behavior described in Scheme 4, we find that both *cis*- and *trans*-(ligand)^{X}PtCl$_2$ form the *cis*-(ligand)Pt product upon treatment with four equivalents of *s*BuLi. The configuration of this product was deduced from the $^1J_{P,Pt}$ coupling constant of about 2000 Hz and the $^2J_{P,C}$ coupling constants of about 10 Hz for the *cis* coupling and about 105 Hz for the *trans* coupling (cf. *cis*-[**2**]PtEt$_2$: $^2J_{C,Pcis}$ = 8.1, $^2J_{C,Ptrans}$ = 110.5 Hz and *cis*-[**3**]PtEt$_2$: $^2J_{C,Pcis}$ = 10.7, $^2J_{C,Ptrans}$ = 113.4 Hz). The question to be examined for the *cis*-(ligand)Pt complexes was how they behave under the thermolysis conditions employed for *cis*-(ligand)PtEt$_2$ (80–100 °C, ethene present).

cis-[**3***]Pt isomerizes slowly and quantitatively at 95 °C in toluene (with and without ethene) to give *trans*-[**3***]Pt (δ_{trans} = 122.1 ppm, $^1J_{Pt,P}$ = 3038.1 Hz). Variable-temperature measurements by ^{1}H NMR spectroscopy between –90 °C and 100 °C in toluene indicate a dynamic process in *cis*-[**3***]-Pt [broadening of the OCH_2 protons and the *i*Pr groups; line shape analysis: $\Delta H^{\neq}$ = 7.6 kcal mol^{-1}, $\Delta S^{\neq}$ = –14.6 cal mol^{-1} K^{-1}, coalescence point 0 °C; Figure 11 (left)]. Since no line broadening is observed in the ^{31}P NMR spectrum we can conclude that the phosphorus atoms remain coordinated during the dynamic process, which we assign to restricted conformational change of the chelating six-membered rings.

This is supported by the X-ray structure of a molecule in the solid state (Figure 12, Table 6). P1, P2, Pt1, C6, and C7 are almost in one plane in *cis*-[**3***]Pt and the P–Pt–P angle is 105° (larger than 90°). The distance between the "cleaved" C atoms C6 and C7 is 2.8 Å and the C6–Pt–C7 angle is 85°.

The same kind of broadening is observed in the ^{1}H NMR spectrum of *trans*-[**3***]Pt [broadening of the OCH_2 protons and the *i*Pr groups; line shape analysis: $\Delta H^{\neq}$ = 6.1 kcal mol^{-1}, $\Delta S^{\neq}$ = –20.5 cal mol^{-1} K^{-1}, coalescence point 0 °C; Figure 11 (right)]. These are the only changes taking place. No back reaction to [**3**]Pt(ethene) or [**3**]Pt is found up to 150 °C in mesitylene under ethene atmosphere either for the *cis*- or for the *trans* complex.

cis-[**1***]Pt is slowly and quantitatively transformed into two new products when heated to 95 °C. One of these has

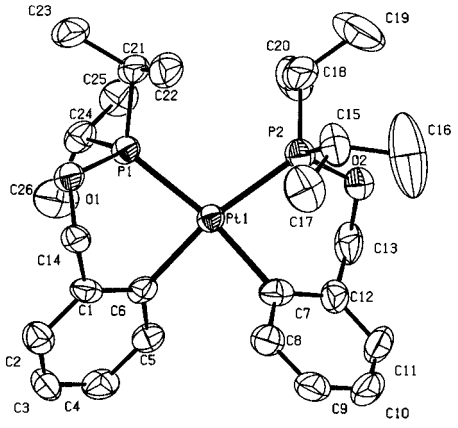

Figure 12. ORTEP style plot of the compound *cis*-[**3***]Pt in the solid. Thermal ellipsoids are drawn at the 50% probability level. Hydrogen atoms have been omitted for clarity.

Table 6. Geometric data for three (ligand)Pt compounds as determined by X-ray analysis.

	cis-[**1***]Pt	*trans*-[**1***]Pt	*cis*-[**3***]Pt
Pt–P2 [Å]	2.2756(7)	2.2611(12)	2.294(3)
Pt–P3 [Å]	2.2726(7)	2.2611(12)	2.297(3)
Pt–C4 [Å]	2.070(3)	2.094(2)	2.069(10)
Pt–C5 [Å]	2.083(3)	2.094(2)	2.080(11)
C_a–C_b (bridge) [Å]	3.063(4)	–	2.806(16)
P–Pt–P [°]	108.44(3)	180	105.0(1)
alk–Pt–alk [°]	95.04(11)	180	85.1(4)

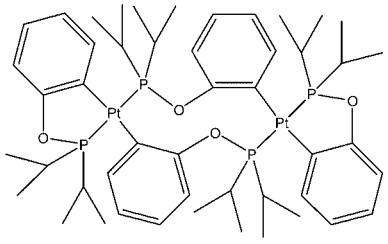

Figure 13. Proposed structure of the second product found in the course of *cis*/*trans* isomerization of *cis*-[**1***]Pt based on the ^{31}P NMR results.

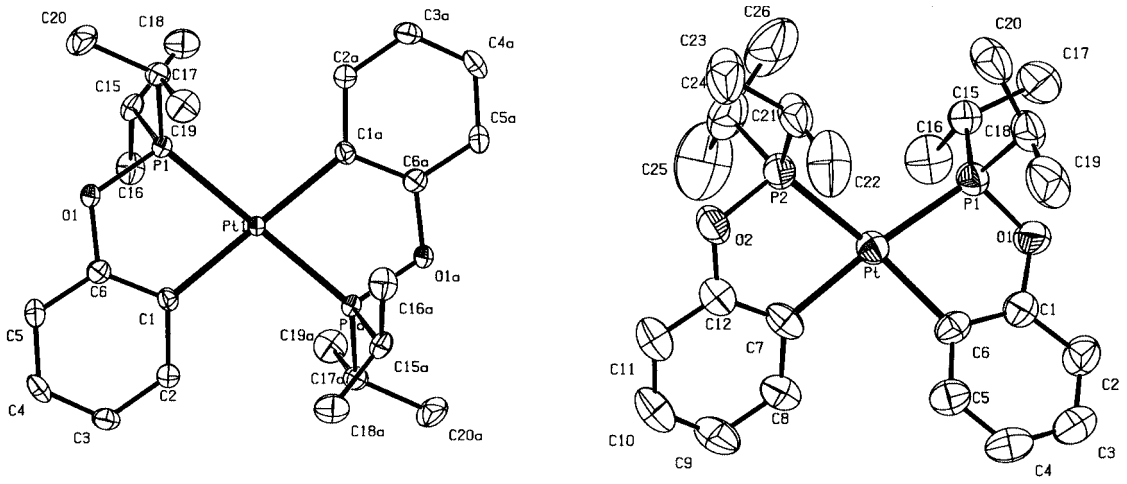

Figure 14. ORTEP style plot of the compounds *trans*-[**1***]Pt (left) and *cis*-[**1***]Pt (right) in the solid. Thermal ellipsoids are drawn at the 50% probability level. Hydrogen atoms have been omitted for clarity.

equivalent P atoms and the other one has inequivalent ones (all of them bound to Pt) and they are formed regardless of whether the reaction is performed under an atmosphere of argon or ethene. The product with equivalent P atoms is *trans*-[**1***]Pt, which was isolated and single crystals were grown from toluene solution. We assume the second product to be a *trans*-configured dimer (Figure 13), although we could not support this supposition by FAB mass spectrometry. A *trans* configuration would be in accordance with the $^1J_{P,Pt}$ coupling constants of 3073.6 and 2867.5 Hz and the $^2J_{P,P}$ coupling constant of 439.9 Hz. In this connectivity the two phenyl planes of one Pt center should be oriented perpendicular to each other and thus prevent close contacts with the *i*Pr groups.

X-ray structures of *cis*/*trans*-[**1***]Pt were determined and are shown in Figure 14 (Table 6). In contrast to *trans*-[**1***]-Pt, which is almost square planar, *cis*-[**1***]Pt is significantly distorted out of the square plane, most probably to avoid close contacts between the two *i*Pr groups and/or the two *ortho* protons in the phenyl groups. Compound **d** of Scheme 1 ([**1**]Pt(ethene)) is not observed in the course of the *cis*/*trans* isomerization, thus demonstrating that both the *cis*- and *trans*-[**1***]Pt complexes are stable or inert against a reductive elimination and should thus be observable if formed in the course of the reactions proposed in Scheme 1.

Conclusions

We have been able to push our master plan to activate and cleave a C–C single bond in a non-strained biphenyl fragment one step further (loss of the alkene) by allowing the backbone of the chelating ligand to be more flexible, although we have still not been able to reach our final target. We have shown that loss of the alkene is not the limiting factor and we have found convincing evidence that a dynamic C–H activation of the methyl groups in the *i*Pr substituents of the chelating ligand prevents a further reaction of the 14e intermediate, especially a potential activation of the bridging C–C single bond in the biphenyl fragment of the chelating ligand. We have also proved that the potential C–C single bond activation products are stable (or inert) under the reaction conditions employed. The scrambling of deuterium into the methyl groups of the ligand in the course of thermolysis underlines the ability of the intermediate to activate less reactive bonds. Although the investigation of the dynamic C–H activation is an interesting exercise, this is not our main target. One solution to successfully finish our strategy might be to exchange the H atoms in the *i*Pr methyl groups by F atoms. Preliminary attempts in this direction have shown that the synthesis of the fluorinated ligand will be tedious and expensive. The exchange of our oxo group for a CH_2 might be advantageous too.[4m] Detailed DFT calculations in order to determine the C–C single bond activation barrier are also underway.

Experimental Section

Manipulations and experiments were performed under argon using standard Schlenk techniques and/or in an argon-filled glove-box if not mentioned otherwise. Diethyl ether, pentane, acetonitrile, dichloromethane, toluene and thf were dried and degassed using a two-column drying system (MBraun) and stored under argon over molecular sieves. $CDCl_3$, [D_8]toluene, and [D_5]pyridine were stored under argon over molecular sieves. Ethene 2.7, H_2 5.0, and D_2 2.7 were purchased from Messer Grießheim and used as delivered. K_2PtCl_4 was purchased from Strem Chemicals and used without further manipulation. (1*Z*,5*Z*)-cyclooctadiene (COD), chlorodiphenylphosphane, chlorodiisopropylphosphane, 2,2′-dihydroxybiphenyl, 2,2′-biphenylmethanol, biphenic acid, *n*-propyl- and ethylmagnesium chloride (2 M in diethyl ether), CD_3CD_2Br, $LiAlH_4$, $LiAlD_4$, and chloroperoxobenzoic acid were purchased from Aldrich and used without further purification. [(COD)$PtCl_2$] and *trans*-[$PtCl_2$(ethene)(py)] were synthesized according to the literature.[10]

NMR spectra were recorded on a Bruker AMX400. ^1H (δ = 7.24 ppm, 400 MHz) and ^{13}C (δ = 77.0 ppm, 100 MHz) were referenced to the $CDCl_3/CHCl_3$ resonances, ^{31}P (161 MHz) to 85% H_3PO_4 as external standard, and ^{195}Pt (δ = –3329 ppm, 85.6 MHz) to [(COD)$PtCl_2$] as external standard. FTIR spectra were recorded

with a JASCO FI7IR-460plus machine using KBr pellets. Variable-temperature measurements were performed as reported previously.[3,11]

Benzo[*c*]chromen-6-one: Fluoren-9-one (1.0 g, 5.55 mmol) and of *m*-chloroperoxobenzoic acid (1.91 g, at least 77%/8.52 mmol) were dissolved in 12 mL of glacial acetic acid and 2 mL of conc. sulfuric acid and the mixture refluxed for 2 d. After cooling to room temperature, 200 mL of diethyl ether was added followed by a saturated sodium sulfite solution to destroy the unreacted peroxide until no more gas evolution was observed. The organic phase was then washed with a saturated sodium carbonate solution until the water phase was clear and slightly basic. The light yellow ether phase was washed with 100 mL of distilled water, dried with $MgSO_4$, and the solvent was removed in vacuo to give 0.86 g (4.38 mmol, 79%) of the pure product as a yellow solid. ^{1}H NMR ($CDCl_3$): δ = 7.35 (t, $^3J_{H,H}$ = 9.8 Hz, 2 H, CH arom.), 7.49 (m, 1 H, CH arom.), 7.63 (m, 1 H, CH arom.), 7.87 (t, $^3J_{H,H}$ = 7.4 Hz, 1 H, CH arom.), 8.04 (d, $^3J_{H,H}$ = 7.4 Hz, 1 H, CH arom.), 8.11 (d, $^3J_{H,H}$ = 7.4 Hz, 1 H, CH arom.), 8.40 (d, $^3J_{H,H}$ = 9.8 Hz, 1 H, CH arom.) ppm. ^{13}C{^{1}H} NMR ($CDCl_3$): δ = 117.8 (s, CH arom.), 118.1 (s, CH arom.), 121.3 (s, CH arom.), 121.7 (s, CH arom.), 122.8 (s, CH arom.), 124.5 (s, CH arom.), 128.9 (s, CH arom.), 130.4 (s, CH arom.), 130.6 (s, CH arom.), 134.8 (s, CH arom.), 135.6 (s, CH-arom.), 151.3 (s, CH arom.), 161.2 (s, -CO-) ppm.

2-Hydroxy-2′-(hydroxymethyl)biphenyl: Lithium aluminum hydride (0.58 g, 15.3 mmol) was suspended in 100 mL of diethyl ether in a 500-mL, two-necked vessel equipped with a condenser and dropping funnel and of benzo[*c*]chromen-6-one (1.0 g, 5.10 mmol) in 100 mL of diethyl ether was dropwise added while stirring. The mixture was then refluxed in a water bath for 3.5 h. After cooling to 0 °C the grey suspension was treated slowly with 100 mL of cold water, then 0.1 M aqueous HCl was added until the grey precipitate had dissolved completely. The yellow organic phase was separated and the water phase was extracted three times with 100 mL of diethyl ether. The combined organic phases were dried with $MgSO_4$ and the solvent was removed in vacuo. The light brownish solid was recrystallized from methanol. Yield: 94%. ^{1}H NMR ($CDCl_3$): δ = 2.18 (br. s, 1 H, -CH_2-O*H*), 4.48 (s, 2 H, -C*H*$_2$-), 5.76 (br. s, 1 H, benzyl-OH), 6.97 (m, 2 H, CH arom.), 7.10 (m, 1 H, CH arom.), 7.26 (m, 2 H, CH arom.), 7.38–7.44 (m, 2 H, CH arom.), 7.53 (m, 1 H, CH arom.) ppm. ^{13}C{^{1}H} NMR ($CDCl_3$): δ = 63.7 (s, CH arom.), 116.4 (s, CH arom.), 120.9 (s, CH arom.), 127.6 (s, CH arom.), 128.6 (s, CH arom.), 128.7 (s, CH arom.), 129.3 (s, CH arom.), 129.4 (s, CH arom.), 130.7 (s, CH arom.), 130.9 (s, CH arom.), 136.3 (s, CH arom.), 138.9 (s, CH arom.), 152.8 (s, -CO-) ppm.

2-(Diisopropylphosphanyloxy)-2′-[(diisopropylphosphanyl)oxymethyl]biphenyl (2): The synthesis was performed according to our previous published procedure.[3] Colorless oil, yield: 75%. ^{1}H NMR ($CDCl_3$): δ = 0.71–1.33 (m, 28 H, CHC*H*$_3$), 1.57–1.76 (m, 4 H, C*H*CH$_3$), 4.46 (m, 2 H, CH_2), 7.00 (d, $^3J_{H,H}$ = 7.4 Hz, 1 H, CH arom.), 7.16 (m, 2 H, CH arom.), 7.26–7.36 (m, 4 H, CH arom.), 7.58 (d, $^3J_{H,H}$ = 7.4 Hz, 1 H, CH arom.) ppm. ^{13}C{^{1}H} NMR ($CDCl_3$): δ = 17.9 (d, $^2J_{C,P}$ = 19.6 Hz, CH*C*H$_3$), 28.0 (d, $^1J_{C,P}$ = 16.8 Hz, *C*HCH$_3$), 72.0 (d, $^2J_{C,P}$ = 21.2 Hz, CH_2), 117.2 (s, CH arom.), 117.4 (s, CH arom.), 121.2 (s, CH arom.), 126.6 (s, CH arom.), 126.9 (s, CH arom.), 127.1 (s, CH arom.), 130.3 (s, CH arom.), 130.9 (s, CH arom.), 137.0 (s, CH arom.), 138.3 (d, $^3J_{C,P}$ = 8.8 Hz, *C*-CH_2OP), 155.8 (d, $^2J_{C,P}$ = 8.1 Hz, COP) ppm. ^{31}P{^{1}H} NMR ($CDCl_3$): δ = 155.0 (s), 158.3 (s) ppm.

2,2′-Bis[(diisopropylphosphanyl)oxymethyl]biphenyl (3): The synthesis was performed according to our previous published procedure.[3] Clear oily liquid, yield: 70%. ^{1}H NMR ($CDCl_3$): δ = 0.91–1.04 (m, 28 H, CHC*H*$_3$), 1.68 (sept, $^2J_{H,H}$ = 7.4 Hz, 4 H, CHCH$_3$), 4.42 (d, $^2J_{H,H}$ = 12.3 Hz, 1 H, -CH_2-), 4.47 (d, $^2J_{H,H}$ = 12.3 Hz, 1 H, -CH_2-), 7.14 (d, $^3J_{H,H}$ = 7.3 Hz, 2 H, 1 H, CH arom.), 7.29 (d, $^3J_{H,H}$ = 7.3 Hz, 1 H, CH-arom.), 7.31 (d, $^3J_{H,H}$ = 7.4 Hz, 1 H, CH arom.), 7.36 (d, $^3J_{H,H}$ = 7.3 Hz, 1 H, CH arom.), 7.38 (d, $^3J_{H,H}$ = 7.4 Hz, 1 H, CH arom.), 7.57 (d, $^3J_{H,H}$ = 7.3 Hz, 2 H, CH arom.) ppm. ^{13}C{^{1}H} NMR ($CDCl_3$): δ = 16.9 (d, $^2J_{C,P}$ = 8.1 Hz, CH*C*H$_3$), 17.0 (d, $^2J_{C,P}$ = 8.8 Hz, CH*C*H$_3$), 17.7 (d, $^2J_{C,P}$ = 6.6 Hz, CH*C*H$_3$), 17.9 (d, $^2J_{C,P}$ = 6.6 Hz, CH*C*H$_3$), 27.9 (d, $^2J_{C,P}$ = 16.1 Hz, *C*HCH$_3$), 28.1 (d, $^2J_{C,P}$ = 16.1 Hz, *C*HCH$_3$), 71.9 (d, $^2J_{C,P}$ = 20.5 Hz, CH_2OP), 127.0 (s, CH arom.), 127.6 (s, CH arom.), 128.1 (s, CH arom.), 129.6 (s, CH arom.), 137.3 (d, $^3J_{C,P}$ = 8.8 Hz, *C*-CH_2-O), 138.8 (s, CH arom.) ppm. ^{31}P{^{1}H} NMR ($CDCl_3$): δ = 154, 4 (s) ppm.

Synthesis of the Dichloridodiphosphinite Complexes. General Procedure for the Synthesis of the Complexes [Y]PtCl$_2$ (Y = 2, 3): A solution of 0.3 mmol of ligand Y in 5 mL of dichloromethane was added with a syringe to a suspension of 0.3 mmol of precursor in 20 mL of dichloromethane. The mixture was stirred overnight at room temperature and the solvent was then removed in vacuo. The white to light-yellow residue was washed with 10 mL of pentane (in some cases additionally with 4 mL of diethyl ether) and dried for 2 h in vacuo. Recrystallization from dichloromethane was necessary to give analytically pure material.

***cis*-[2]PtCl$_2$:** Light-yellow powder, yield: 70%. ^{1}H NMR ($CDCl_3$): δ = 0.63 (d, $^3J_{H,H}$ = 7.8 Hz, 3 H, CHC*H*$_3$), 0.65 (d, $^3J_{H,H}$ = 6.9 Hz, 3 H, CHC*H*$_3$), 0.88 (d, $^3J_{H,H}$ = 7.8 Hz, 3 H, CHC*H*$_3$), 0.92 (d, $^3J_{H,H}$ = 6.8 Hz, 3 H, CHC*H*$_3$), 0.98 (d, $^3J_{H,H}$ = 6.9 Hz, 3 H, CHC*H*$_3$), 1.06 (d, $^3J_{H,H}$ = 7.8 Hz, 3 H, CHC*H*$_3$), 1.45 (d, $^3J_{H,H}$ = 6.9 Hz, 3 H, CHC*H*$_3$), 1.48 (d, $^3J_{H,H}$ = 7.8 Hz, 3 H, CHC*H*$_3$), 2.51 (m, 1 H, C*H*CH$_3$), 2.60 (m, 1 H, C*H*CH$_3$), 2.75 (m, 1 H, C*H*CH$_3$), 3.46 (m, 1 H, C*H*CH$_3$), 4.61 (d, $^3J_{H,H}$ = 8.8 Hz, 1 H, -CH_2-), 4.70 (d, $^3J_{H,H}$ = 6.9 Hz, 1 H, -CH_2-), 7.14–7.50 (m, 8 H, CH arom.) ppm. ^{13}C{^{1}H} NMR ($CDCl_3$): δ = 16.4 (d, $^2J_{C,P}$ = 6.2 Hz, CH*C*H$_3$), 17.1 (d, $^2J_{C,P}$ = 6.2 Hz, CH*C*H$_3$), 17.8 (d, $^2J_{C,P}$ = 2.5 Hz, CH*C*H$_3$), 18.7 (br. d, $^2J_{C,P}$ = 13.3 Hz, CH*C*H$_3$), 19.5 (br.s, CH*C*H$_3$), 20.4 (d, $^2J_{C,P}$ = 3.7 Hz, CH*C*H$_3$), 28.6 (d, $^2J_{C,P}$ = 32.1 Hz, *C*HCH$_3$), 31.0 (d, $^2J_{C,P}$ = 35.7 Hz, *C*HCH$_3$), 31.8 (d, $^2J_{C,P}$ = 35.8 Hz, *C*HCH$_3$), 34.2 (d, $^2J_{C,P}$ = 43.2 Hz, *C*HCH$_3$), 69.2 (d, $^1J_{C,P}$ = 13.6 Hz, CH_2), 119.3 (d, $^4J_{C,P}$ = 6.2 Hz, *C*HCCH$_2$), 123.3 (s, CH arom.), 128.1 (s, CH arom.), 129.4 (s, CH arom.), 129.5 (s, CH arom.), 129.8 (s, CH arom.), 130.3 (s, CH arom.), 132.1 (d, $^3J_{C,P}$ = 6.2 Hz, *C*HCOP), 134.1 (d, $^4J_{C,P}$ = 6.2 Hz, *C*HCCH$_2$), 139.6 (s, CH arom.), 151.9 (d, $^3J_{C,P}$ = 8.6 Hz, C-O-P) ppm. ^{31}P{^{1}H} NMR ($CDCl_3$): δ = 112.5 (pseudo t, $^1J_{P,Pt}$ = 4099.0, $^2J_{P,P}$ = 5.0 Hz), 110.5 (pseudo t, $^1J_{P,Pt}$ = 4149.6, $^2J_{P,P}$ = 5.0 Hz) ppm. ^{195}Pt{^{1}H} NMR ($CDCl_3$): δ = –4116.8 (dd, $^1J_{P,Pt}$ = 4099.0, 4149.6 Hz) ppm. $C_{25}H_{38}Cl_2O_2P_2Pt$ (698.50): calcd. C 42.99, H 5.48, Cl 10.15, P 8.87; found C 43.07, H 5.55, Cl 9.78, P 8.05.

Crystal-Structure Analysis of *cis*-[2]PtCl$_2$·2(CHCl$_3$): $C_{27}H_{40}Cl_8O_2P_2Pt$, M_r = 937.26, colorless fragment ($0.06 \times 0.18 \times 0.12$ mm^3), monoclinic, $P2_1/c$ (no. 14), a = 9.9002(1), b = 17.7053(2), c = 21.2118(3) Å, β = 100.9809(5)°, V = 3650.06(8) Å^3, Z = 4, D_{calc} = 1.706 g cm^{-3}, $F(000)$ = 1848, μ = 4.542 mm^{-1}. Preliminary examination and data collection were carried out on a κ-CCD device (Nonius, Mach3) with an Oxford Cryosystems cooling system at the window of a rotating anode (Nonius FR591) with graphite-monochromated Mo-K_α radiation (λ = 0.71073 Å). Data collection was performed at 173 K within the Θ range $1.51° < \Theta < 25.36°$. A total of 44141 intensities were integrated. Raw data were corrected for Lorentz, polarization, and

latent decay and absorption effects arising from the scaling procedure. After merging (R_{int} = 0.0429), 6670 [5689: $I_0 > 2\sigma(I_0)$] independent reflections remained and all were used to refine 369 parameters. The structure was solved by a combination of direct methods and difference-Fourier syntheses. All non-hydrogen atoms were refined with anisotropic displacement parameters. All hydrogen atoms were placed in calculated positions and refined using a riding model. Full-matrix least-squares refinements were carried out by minimizing $\Sigma w(F_o^2 - F_c^2)^2$ and converged with $R1$ = 0.0380 [$I_0 > 2\sigma(I_0)$], $wR2$ = 0.0702 (all data), GOF = 1.162, and shift/error < 0.001. The final difference-Fourier map showed no striking features ($\Delta e_{min/max}$ = +1.01/–1.02 e Å^{-3}). CCDC-613907.

***cis*-[3]PtCl$_2$:** White powder, yield: 83%. ^{1}H NMR ($CDCl_3$): δ = 0.91 (d, $^3J_{H,H}$ = 7.3 Hz, 3 H, CHC*H*$_3$), 0.95 (d, $^3J_{H,H}$ = 4.9 Hz, 3 H, CHC*H*$_3$), 1.22 (d, $^3J_{H,H}$ = 7.4 Hz, 3 H, CHC*H*$_3$), 1.26 (d, $^3J_{H,H}$ = 7.3 Hz, 3 H, CHC*H*$_3$), 1.32 (d, $^3J_{H,H}$ = 7.4 Hz, 3 H, CHC*H*$_3$), 1.35 (d, $^3J_{H,H}$ = 4.9 Hz, 3 H, CHC*H*$_3$), 1.57 (d, $^3J_{H,H}$ = 7.4 Hz, 3 H, CHC*H*$_3$), 1.62 (d, $^3J_{H,H}$ = 7.4 Hz, 3 H, CHC*H*$_3$), 2.27 (m, 2 H, C*H*CH$_3$), 3.48 (m, 2 H, C*H*CH$_3$), 4.37 (d, $^3J_{H,H}$ = 9.8 Hz, 2 H, CH$_2$), 4.81 (d, $^3J_{H,H}$ = 9.8 Hz, 2 H, CH$_2$), 7.14 (d, $^3J_{H,H}$ = 7.3 Hz, 2 H, CH arom.), 7.21–7.32 (m, 4 H, CH arom.), 7.35 (d, $^3J_{H,H}$ = 7.4 Hz, 2 H, CH arom.) ppm. ^{13}C{^{1}H} NMR ($CDCl_3$): δ = 17.2 (br. s, CH*C*H$_3$), 17.8 (br. s, CH*C*H$_3$), 18.8 (s, CH*C*H$_3$), 19.2 (s, CH*C*H$_3$), 26.1 (d, $^1J_{C,P}$ = 30.7 Hz, *C*HCH$_3$), 30.2 (d, $^1J_{C,P}$ = 41.7 Hz, *C*HCH$_3$), 68.0 (d, $^2J_{C,P}$ = 13.2 Hz, -CH$_2$-), 128.6 (s, CH arom.), 129.1 (s, CH arom.), 130.4 (s, CH arom.), 134.2 (pseudo t, $^4J_{C,P}$ = 4.4 Hz, *C*CH$_2$OP), 140.2 (s, CH arom.) ppm. ^{31}P{^{1}H} NMR ($CDCl_3$): δ = 115.7 (br. pseudo t, $^1J_{P,Pt}$ = 4267.2 Hz) ppm. ^{195}Pt{^{1}H} NMR ($CDCl_3$): δ = –4223.4 (t, $^1J_{P,Pt}$ = 4267.2 Hz) ppm. $C_{26}H_{40}Cl_2O_2P_2Pt$ (712.52): calcd. C 43.83, H 5.66, Cl 8.69, P 9.95; found C 43.71, H 5.69, Cl 8.40, P 9.95.

Crystal-Structure Analysis of *cis*-[3]PtCl$_2$·3(CHCl$_3$): $C_{29}H_{43}Cl_{11}O_2P_2Pt$, M_r = 1070.66, colorless fragment (0.18 × 0.21 × 0.33 mm^3), monoclinic, *C*2/*c* (no. 15), *a* = 32.6825(2), *b* = 19.3448(2), *c* = 21.0863(2) Å, β = 120.9619(4)°, *V* = 11431.91(18) Å^3, *Z* = 8, D_{calc} = 1.658 g cm^{-3}, *F*(000) = 5640, μ = 4.352 mm^{-1}. Preliminary examination and data collection were carried out on a κ-CCD device (Nonius, Mach3) with an Oxford Cryosystems cooling system at the window of a rotating anode (Nonius FR591) with graphite-monochromated Mo-K_α radiation (λ = 0.71073 Å). Data collection was performed at 173 K within the Θ range 1.28° < Θ < 23.27°. A total of 37465 intensities were integrated. Raw data were corrected for Lorentz, polarization, and latent decay and absorption effects arising from the scaling procedure. After merging (R_{int} = 0.0437), 8197 [6947: $I_0 > 2\sigma(I_0)$] independent reflections remained and all were used to refine 247 parameters. The structure was solved by a combination of direct methods and difference-Fourier syntheses. All non-hydrogen atoms were refined with anisotropic displacement parameters. All hydrogen atoms were placed in calculated positions and refined using a riding model. Full-matrix least-squares refinements were carried out by minimizing $\Sigma w(F_o^2 - F_c^2)^2$ and converged with $R1$ = 0.0405 [$I_0 > 2\sigma(I_0)$], $wR2$ = 0.0783 (all data), GOF = 1.089, and shift/error < 0.001. The final difference-Fourier map showed no striking features ($\Delta e_{min/max}$ = +0.85/–0.58 e Å^{-3}). CCDC-613913.

***trans*-[2]PtCl$_2$:** Light-yellow powder, yield: 59%. ^{1}H NMR ($CDCl_3$): δ = 1.04 (d, $^3J_{H,H}$ = 7.4 Hz, 3 H, CHC*H*$_3$), 1.09 (d, $^3J_{H,H}$ = 7.4 Hz, 3 H, CHC*H*$_3$), 1.15–1.25 (m, 6 H, CHC*H*$_3$), 1.31 (pseudo t, $^3J_{H,H}$ = 7.4 Hz, 6 H, CHC*H*$_3$), 1.47 (d, $^3J_{H,H}$ = 7.4 Hz, 3 H, CHC*H*$_3$), 1.50 (d, $^3J_{H,H}$ = 12.3 Hz, 3 H, CHC*H*$_3$), 2.90 (m, 3 H, C*H*CH$_3$), 3.23 (s, $^3J_{H,H}$ = 7.4 Hz, 1 H, C*H*CH$_3$), 4.89 (dd, $^3J_{P,H}$ = 27.0, $^2J_{H,H}$ = 12.3 Hz, 1 H, CH$_2$), 5.35 (dd, $^3J_{P,H}$ = 7.4, $^2J_{H,H}$ = 12.3 Hz, 1 H, -CH$_2$-), 6.87 (d, $^3J_{H,H}$ = 7.4 Hz, 1 H, CH arom.), 7.00 (d, $^3J_{H,H}$ = 9.8 Hz, 1 H, CH arom.), 7.11 (pseudo t, $^3J_{H,H}$ = 7.4 Hz, 2 H, CHC*H*$_3$), 7.23 (m, 1 H, CH arom.), 7.33 (m, 2 H, CH arom.), 7.49 (d, $^3J_{H,H}$ = 7.4 Hz, 1 H, CH arom.) ppm. ^{13}C{^{1}H} NMR ($CDCl_3$): δ = 15.8 (d, $^2J_{C,P}$ = 2.2 Hz, CH*C*H$_3$), 16.1 (s, CH*C*H$_3$), 16.3 (d, $^2J_{C,P}$ = 2.2 Hz, CH*C*H$_3$), 16.9 (d, $^2J_{C,P}$ = 5.1 Hz, CH*C*H$_3$) 17.3 (s, CH*C*H$_3$), 17.5 (s, CH*C*H$_3$), 17.6 (s, CH*C*H$_3$), 18.0 (d, $^2J_{C,P}$ = 4.4 Hz, CH*C*H$_3$), 24.6 (d, $^1J_{C,P}$ = 23.4 Hz, *C*HCH$_3$), 24.9 (d, $^1J_{C,P}$ = 31.5 Hz, *C*HCH$_3$), 25.1 (d, $^1J_{C,P}$ = 27.2 Hz, *C*HCH$_3$), 25.6 (d, $^1J_{C,P}$ = 30.7 Hz, *C*HCH$_3$), 67.7 (d, $^2J_{C,P}$ = 13.2 Hz, CH$_2$), 123.4 (s, CH arom.), 123.8 (s, CH arom.), 127.0 (s, CH arom.), 128.0 (s, CH arom.), 128.6 (s, CH arom.), 129.3 (s, CH arom.), 131.0 (s, CH arom.), 132.7 (s, CH arom.), 133.6 (s, CH arom.), 133.6 (s, CH arom.), 138.8 (s, CH arom.), 150.8 (d, $^3J_{C,P}$ = 7.3 Hz, C-O-P) ppm. ^{31}P{^{1}H} NMR ($CDCl_3$): δ = 109.3 (d pseudo t, $^2J_{P,P}$ = 488.5 Hz, $^1J_{P,Pt}$ = 2624.9 Hz), 118.8 (d pseudo t, $^2J_{P,P}$ = 488.5, $^1J_{P,Pt}$ = 2690.7 Hz) ppm. ^{195}Pt{^{1}H} NMR ($CDCl_3$): δ = –3805.7 ppm (dd, $^1J_{P,Pt}$ = 2624.9, $^1J_{P,Pt}$ = 2690.7 Hz). $C_{25}H_{38}Cl_2O_2P_2Pt$ (698.50): calcd. C 42.99, H 5.48, Cl 10.15, P 8.87; found C 43.15, H 5.61, Cl 9.48, P 8.10.

Crystal-Structure Analysis of *trans*-[2]PtCl$_2$: $C_{25}H_{38}Cl_2O_2P_2Pt$, M_r = 698.50, pale-yellow plate (0.05 × 0.10 × 0.26 mm^3), triclinic, $P\bar{1}$ (no. 2), *a* = 10.4738(1), *b* = 16.4348(1), *c* = 17.7791(2) Å, α = 11.7991(5)°, β = 100.3275(4)°, γ = 97.7027(4)°, *V* = 2727.71(4) Å^3, *Z* = 4, D_{calc} = 1.701 g cm^{-3}, *F*(000) = 1384, μ = 5.477 mm^{-1}. Preliminary examination and data collection were carried out on a κ-CCD device (Nonius, Mach3) with an Oxford Cryosystems cooling system at the window of a rotating anode (Nonius FR591) with graphite-monochromated Mo-K_α radiation (λ = 0.71073 Å). Data collection was performed at 173 K within the Θ range 1.27° < Θ < 25.42°. A total of 62373 intensities were integrated. Raw data were corrected for Lorentz, polarization, and latent decay and absorption effects arising from the scaling procedure. After merging (R_{int} = 0.0257), 10013 [8464: $I_0 > 2\sigma(I_0)$] independent reflections remained and all were used to refine 593 parameters. The structure was solved by a combination of direct methods and difference-Fourier syntheses. All non-hydrogen atoms were refined with anisotropic displacement parameters. All hydrogen atoms were placed in calculated positions and refined using a riding model. Full-matrix least-squares refinements were carried out by minimizing $\Sigma w(F_o^2 - F_c^2)^2$ and converged with $R1$ = 0.0336 [$I_0 > 2\sigma(I_0)$], $wR2$ = 0.0832 (all data), GOF = 1.132, and shift/error < 0.001. The final difference-Fourier map showed no striking features ($\Delta e_{min/max}$ = +1.32/–1.49 e Å^{-3}). CCDC-613904.

***trans*-[3]PtCl$_2$:** White powder, yield: 61%. ^{1}H NMR ($CDCl_3$): δ = 1.18–1.27 (m, 18 H, CHC*H*$_3$), 1.36 (d, $^3J_{H,H}$ = 7.0 Hz, 3 H, CHC*H*$_3$), 1.41 (d, $^3J_{H,H}$ = 7.1 Hz, 3 H, CHC*H*$_3$), 2.90–3.05 (m, 4 H, C*H*CH$_3$), 4.83 (pseudo t, $^2J_{H,H}$ = $^3J_{P,H}$ = 8.3 Hz, 2 H, -CH$_2$-), 4.87 (pseudo t, $^2J_{H,H}$ = $^3J_{P,H}$ = 8.3 Hz, 2 H, -CH$_2$-), 5.59 (pseudo t, $^2J_{H,H}$ = $^3J_{P,H}$ = 8.3 Hz, 2 H, -CH$_2$-), 5.62 (pseudo t, $^2J_{H,H}$ = $^3J_{P,H}$ = 8.3 Hz, 2 H, -CH$_2$-), 6.96 (d, $^3J_{H,H}$ = 7.4 Hz, 2 H, CH arom.), 7.25 (m, 2 H, CH arom.), 7.38 (d, $^3J_{H,H}$ = 7.1 Hz, 1 H, CH arom.), 7.40 (d, $^3J_{H,H}$ = 7.6 Hz, 1 H, CH arom.), 7.58 (d, $^3J_{H,H}$ = 7.6 Hz, 2 H, CH arom.) ppm. ^{13}C{^{1}H} NMR ($CDCl_3$): δ = 16.5 (s, CH*C*H$_3$), 16.9 (s, CH*C*H$_3$), 17.3 (s, CH*C*H$_3$), 17.4 (s, CH*C*H$_3$), 25.3 (d, $^1J_{C,P}$ = 35.5 Hz, *C*HCH$_3$), 25.5 (d, $^1J_{C,P}$ = 32.2 Hz, *C*HCH$_3$), 68.4 (s, -CH$_2$-), 122.7 (s, CH arom.), 126.6 (s, CH arom.), 127.7 (s, CH arom.), 129.7 (s, CH arom.), 136.9 (s, CH arom.), 137.5 (s, CH arom.) ppm. ^{31}P{^{1}H} NMR ($CDCl_3$): δ = 118.4 (pseudo t, $^1J_{P,Pt}$ = 2627.5 Hz) ppm. ^{195}Pt{^{1}H} NMR ($CDCl_3$): δ = –3763.1 (t, $^1J_{P,Pt}$ = 2627.5 Hz) ppm. $C_{26}H_{40}Cl_2O_2P_2Pt$ (712.53): calcd. C 43.83, H 5.66, Cl 9.95, P 8.69; found C 43.53, H 5.73, Cl 9.80, P 7.81.

Crystal-Structure Analysis of *trans*-[3]PtCl$_2$: $C_{26}H_{40}Cl_2O_2P_2Pt$, M_r = 712.53, pale-yellow plate (0.15 × 0.21 × 0.46 mm^3), monoclinic, $P2_1/n$ (no. 14), a = 14.8880(2), b = 11.2034(2), c = 17.3298(2) Å, β = 94.4762(9)°, V = 2881.73(7) Å^3, Z = 4, D_{calc} = 1.698 g cm^{-3}, $F(000)$ = 1464, μ = 5.190 mm^{-1}. Preliminary examination and data collection were carried out on a κ-CCD device (Nonius, Mach3) with an Oxford Cryosystems cooling system at the window of a rotating anode (Nonius FR591) with graphite-monochromated Mo-K_α radiation (λ = 0.71073 Å). Data collection was performed at 173 K within the Θ range 1.74° < Θ < 25.34°. A total of 25293 intensities were integrated. Raw data were corrected for Lorentz, polarization, and latent decay and absorption effects arising from the scaling procedure. After merging (R_{int} = 0.0286), 5265 [4430: $I_0 > 2\sigma(I_0)$] independent reflections remained and all were used to refine 306 parameters. The structure was solved by a combination of direct methods and difference-Fourier syntheses. All non-hydrogen atoms were refined with anisotropic displacement parameters. All hydrogen atoms were placed in calculated positions and refined using a riding model. Full-matrix least-squares refinements were carried out by minimizing $\Sigma w(F_o^2 - F_c^2)^2$ and converged with $R1$ = 0.0301 [$I_0 > 2\sigma(I_0)$], $wR2$ = 0.0750 (all data), GOF = 1.042, and shift/error < 0.001. The final difference-Fourier map showed no striking features ($\Delta e_{min/max}$ = +0.72/–1.39 e Å^{-3}). CCDC-613906.

Synthesis of the Dialkyldiphosphinite Complexes. General Procedure for the Synthesis of the Complexes [Y]PtR′$_2$ (Y = 1, 1′, 2, 3; R′ = Alkyl): The dichlorido complex (0.15 mmol) was suspended in 10 mL of diethyl ether and cooled to –78 °C. Then, 0.45 mmol of Alkyl-Grignard were added while stirring and it was warmed up to room temperature overnight. The next day, 0.45 mmol of 1,4-dioxane were added, the white residue was filtered through alumina and washed with 10 mL of diethyl ether. The solvent was removed from the ether extracts in vacuo and the resulting solid was dried in vacuo for two hours.

***cis*-[1]Pt(*n*Pr)$_2$:** White powder, yield: 62%. ^{1}H NMR ($CDCl_3$): δ = 0.60 (d, $^2J_{H,H}$ = 7.4 Hz, 3 H, CHCH_3), 0.64 (d, $^2J_{H,H}$ = 7.3 Hz, 3 H, CHCH_3), 0.87 (d, $^2J_{H,H}$ = 7.4 Hz, 3 H, CHCH_3), 0.90 (d, $^2J_{H,H}$ = 4.9 Hz, 3 H, CHCH_3), 0.86–1.13 (m, 10 H, CH_2CH_3), 1.13–1.38 (m, 12 H, CH_2CH_3, CHCH_3), 2.06 (m, 2 H, CHCH$_3$), 2.66 (m, 2 H, CHCH$_3$), 7.01 (d, $^2J_{H,H}$ = 7.4 Hz, 2 H, CH arom.), 7.09 (t, $^2J_{H,H}$ = 7.4 Hz, 2 H, CH arom.), 7.21–7.26 (m, 4 H, CH arom.) ppm. ^{13}C{^{1}H} NMR ($CDCl_3$): δ = 15.5 [s, Pt(CH$_2$)$_2$CH_3], 17.8 (s, $^2J_{C,Pt}$ = 11.7 Hz, PCH$_2$CH_3), 18.6 (s, $^2J_{C,Pt}$ = 11.7 Hz, PCH$_2$CH_3), 24.1 (dd, $^2J_{C,P\text{-}cis}$ = 10.3, $^2J_{C,P\text{-}trans}$ = 105.4, $^1J_{C,Pt}$ = 642.6 Hz, PtCH$_2$), 25.7 (br. s, PtCH$_2$CH$_2$), 31.7 (d, $^1J_{C,P}$ = 9.5, $^1J_{C,Pt}$ = 36.6 Hz, P-CHCH$_3$), 31.9 (d, $^1J_{C,P}$ = 9.5, $^1J_{C,Pt}$ = 36.6 Hz, PCHCH$_3$), 32.2 (m, PCHCH$_3$), 121.3 (s, CH arom.), 123.5 (s, CH arom.), 131.5 (s, CH arom.), 132.4 (s, CH arom.), 153.3 (d, $^1J_{C,P}$ = 4.4 Hz, C-O-P), 153.3 (d, $^1J_{C,P}$ = 5.1 Hz, C-O-P) ppm. ^{31}P{^{1}H} NMR ($CDCl_3$): δ = 153.2 (pseudo t, $^1J_{P,Pt}$ = 1983.1 Hz) ppm. ^{195}Pt{^{1}H} NMR ([D$_8$]toluene): δ = –4561.3 (t, $^1J_{P,Pt}$ = 1983.1 Hz) ppm. $C_{30}H_{50}O_2P_2Pt$ (699.74): calcd. C 51.49, H 7.20; found C 52.05, H 7.12.

Crystal-Structure Analysis of *cis*-[1]Pt(*n*Pr)$_2$: $C_{30}H_{50}O_2P_2Pt$, M_r = 699.74, colorless needle (0.06 × 0.08 × 0.18 mm^3), monoclinic, $C2/c$ (no. 15), a = 14.5639(2), b = 12.4757(3), c = 17.4797(3) Å, β = 108.1046(17)°, V = 3018.73(10) Å^3, Z = 4, D_{calc} = 1.540 g cm^{-3}, $F(000)$ = 1416, μ = 4.778 mm^{-1}. Preliminary examination and data collection were carried out on a κ-CCD device (Nonius, Mach3) with an Oxford Cryosystems cooling system at the window of a rotating anode (Nonius FR591) with graphite-monochromated Mo-K_α radiation (λ = 0.71073 Å). Data collection was performed at 173 K within the Θ range 1.00° < Θ < 25.35°. A total of 11634 intensities were integrated. Raw data were corrected for Lorentz, polarization, and latent decay and absorption effects arising from the scaling procedure. After merging (R_{int} = 0.0190), 2468 [2437: $I_0 > 2\sigma(I_0)$] independent reflections remained and all were used to refine 164 parameters. The structure was solved by a combination of direct methods and difference-Fourier syntheses. All non-hydrogen atoms were refined with anisotropic displacement parameters. All hydrogen atoms were placed in calculated positions and refined using a riding model. Full-matrix least-squares refinements were carried out by minimizing $\Sigma w(F_o^2 - F_c^2)^2$ and converged with $R1$ = 0.0145 [$I_0 > 2\sigma(I_0)$], $wR2$ = 0.0364 (all data), GOF = 1.123, and shift/error < 0.001. The final difference-Fourier map showed no striking features ($\Delta e_{min/max}$ = +0.83/–0.50 e Å^{-3}). CCDC-613912.

***cis*-[2]PtEt$_2$:** Light-yellow powder, yield: 64%. ^{1}H NMR ($CDCl_3$): δ = 0.63 (d, $^3J_{H,H}$ = 7.4 Hz, 3 H, PCHCH_3), 0.66 (d, $^3J_{H,H}$ = 7.4 Hz, 3 H, PCHCH_3), 0.77–1.51 (m, 28 H, PCHCH_3, PtCH_2CH_3), 2.01 (m, 1 H, CHCH$_3$), 2.26 (m, 1 H, CHCH$_3$), 2.41 (m, 1 H, CHCH$_3$), 2.71 (m, 1 H, CHCH$_3$), 4.40 (d, $^3J_{H,H}$ = 9.8 Hz, 1 H, -CH$_2$-), 4.54 (d, $^3J_{H,H}$ = 9.8 Hz, 1 H, -CH$_2$-), 6.95 (t, $^3J_{H,H}$ = 7.4 Hz, 1 H, CH arom.), 7.03 (d, $^3J_{H,H}$ = 7.4 Hz, 1 H CH arom.), 7.10 (d, $^3J_{H,H}$ = 7.4 Hz, 1 H, CH arom.), 7.14–7.28 (m, 4 H, CH arom.), 7.35 (t, $^3J_{H,H}$ = 7.4 Hz, 1 H, CH arom.) ppm. ^{13}C{^{1}H} NMR ($CDCl_3$): δ = 10.1 (dd pseudo t, $^2J_{C,P\text{-}trans}$ = 8.1, $^2J_{C,P\text{-}cis}$ = 110.5, $^1J_{C,Pt}$ = 481.2 Hz, CHCH$_3$), 14.0 (dd pseudo t, $^2J_{C,P\text{-}trans}$ = 6.6, $^2J_{C,P\text{-}cis}$ = 110.5, $^1J_{C,Pt}$ = 553.9 Hz, CHCH$_3$), 15.5 (d pseudo t, $^3J_{C,P}$ = 6.6, $^2J_{C,Pt}$ = 36.9 Hz, PtCH$_2$CH_3), 15.5 (d pseudo t, $^3J_{C,P}$ = 6.6, $^2J_{C,Pt}$ = 38.0 Hz, PtCH$_2$CH_3), 16.7 (s, CHCH$_3$), 16.8 (s, CHCH$_3$), 17.8 (br. s, CHCH$_3$), 18.3 (br. s, CHCH$_3$), 18.7 (pseudo t, $^3J_{C,P}$ = 10.2 Hz, CHCH$_3$), 19.8 (pseudo t, $^3J_{C,P}$ = 9.8 Hz, CHCH$_3$), 27.1 (d, $^1J_{C,P}$ = 13.2 Hz, CHCH$_3$), 28.2 (d, $^1J_{C,P}$ = 15.4 Hz, CHCH$_3$), 29.4 (d, $^1J_{C,P}$ = 43.2 Hz, CHCH$_3$), 33.9 (d, $^1J_{C,P}$ = 28.5 Hz, CHCH$_3$), 67.1 (d, $^2J_{C,P}$ = 6.6 Hz,CH$_2$), 119.3 (d, $^3J_{C,P}$ = 6.6 Hz, CCCH$_2$OP.), 120.9 (s, CH arom.), 127.2 (s, CH arom.), 128.2 (s, CH arom.), 128.6 (s, CH arom.), 128.8 (s, CH arom.), 128.9 (s, CH arom.), 130.3 (s, CH arom.), 132.8 (d, $^3J_{C,P}$ = 3.7 Hz, CCOP.), 136.4 (d, $^3J_{C,P}$ = 6.6 Hz, CCH$_2$OP), 140.7 (s, CH arom.), 154.2 (d, $^2J_{C,P}$ = 3.7 Hz, COP) ppm. ^{31}P{^{1}H} NMR ($CDCl_3$): δ = 135.0 (d pseudo t, $^2J_{P,P}$ = 17.8, $^1J_{P,Pt}$ = 2008.0 Hz), 110.5 (d pseudo t, $^2J_{P,P}$ = 17.8, $^1J_{P,Pt}$ = 1894.2 Hz) ppm. ^{195}Pt{^{1}H} NMR ([D$_8$]toluene): δ = –4456.0 (dd, $^1J_{P,Pt}$ = 1894.2, $^1J_{P,Pt}$ = 2008.0 Hz) ppm. $C_{29}H_{48}O_2P_2Pt$ (685.72): calcd. C 50.80, H 7.06; found C 50.94, H 7.20.

***cis*-[3]PtEt$_2$:** White powder, yield: 66%. ^{1}H NMR ($CDCl_3$): δ = 0.71 (d, $^3J_{H,H}$ = 7.4 Hz, 3 H, CHCH_3), 0.75 (d, $^3J_{H,H}$ = 7.4 Hz, 3 H, CHCH_3), 0.80–1.12 (m, 14 H, CHCH_3, -CH_2-CH_3), 1.31 (d, $^3J_{H,H}$ = 7.3 Hz, 3 H, CHCH_3), 1.33 (d, $^3J_{H,H}$ = 4.9 Hz, 3 H, CHCH_3), 1.40 (d, $^3J_{H,H}$ = 4.9 Hz, 3 H, CHCH_3), 1.44 (d, $^3J_{H,H}$ = 7.4 Hz, 3 H, CHCH_3), 2.27 (m, 2 H, CHCH$_3$), 2.53 (m, 2 H, CHCH$_3$), 4.33 (d, $^3J_{H,H}$ = 9.8 Hz, 2 H, CH$_2$), 4.61 (d, $^3J_{H,H}$ = 9.8 Hz, 2 H, CH$_2$), 7.08 (d, $^3J_{H,H}$ = 9.8 Hz, 2 H, CH arom.), 7.32 (t, $^3J_{H,H}$ = 7.4 Hz, 2 H, CH arom.), 7.37 (t, $^3J_{H,H}$ = 7.4 Hz, 2 H, CH arom.), 7.50 (d, $^3J_{H,H}$ = 9.8 Hz, 2 H, CH arom.) ppm. ^{13}C{^{1}H} NMR ($CDCl_3$): δ = 12.8 (dd pseudo t, $^2J_{C,P\text{-}cis}$ = 10.7, $^2J_{C,P\text{-}trans}$ = 113.4, $^1J_{C,Pt}$ = 626.4 Hz, Pt-CH$_2$CH$_3$), 15.3 (pseudo t, $^2J_{C,Pt}$ = 5.8 Hz, PtCHCH$_3$), 17.5 (pseudo t, $^2J_{C,Pt}$ = 5.8 Hz, PCHCH$_3$), 18.3 (pseudo t, $^3J_{C,Pt}$ = 5.8 Hz, PCHCH$_3$), 19.0 (d, $^2J_{C,Pt}$ = 7.4 Hz, PCHCH$_3$), 19.1 (d, $^2J_{C,Pt}$ = 6.6 Hz, PCHCH$_3$), 19.4 (br.s, PCH$_2$CH_3) 26.0 (pseudo t, $^1J_{C,P}$ = 7.3, $^2J_{C,Pt}$ = 36.1 Hz, CHCH$_3$), 26.9 (d pseudo t, $^1J_{C,P}$ = 10.0, $^2J_{C,Pt}$ = 47.2 Hz, CHCH$_3$), 27.0 (d pseudo t, $^1J_{C,P}$ = 9.5, $^2J_{C,Pt}$ = 47.3 Hz, CHCH$_3$), 68.3 (d, $^2J_{C,P}$ = 6.6 Hz, -CH$_2$-), 66.5 (d, $^2J_{C,P}$ = 7.3 Hz, -CH$_2$-), 127.9 (s, CH arom.), 128.0 (s, CH arom.), 129.6 (s, CH arom.), 130.6 (s, CH arom.), 136.4 (pseudo t, $^3J_{C,P}$ = 3.7 Hz, CH$_2$OP), 136.5 (pseudo t, $^3J_{C,P}$ = 2.9 Hz, CH$_2$OP), 140.6 (s) ppm.

$^{31}P\{^1H\}$ NMR ($CDCl_3$): δ = 133.6 (pseudo t, $^1J_{P,Pt}$ = 2099.9 Hz) ppm. $^{195}Pt\{^1H\}$ NMR ($CDCl_3$): δ = –4633.4 (t, $^1J_{P,Pt}$ = 2099.9 Hz) ppm. MS (FAB): *m*/*z* (%) 641.3 (100) [M – (ethane + ethene)] (with correct isotope pattern for $C_{26}H_{40}O_2P_2Pt$). $C_{30}H_{50}O_2P_2Pt$: calcd. C 51.49, H 7.20; found C 51.35, H 7.23.

Crystal-Structure Analysis of *cis*-[3]PtEt$_2$: $C_{30}H_{50}O_2P_2Pt$, M_r = 699.74, colorless needle (0.10 × 0.12 × 0.33 mm^3), monoclinic, *P*2/c (no. 13), a = 15.3987(1), b = 12.8649(1), c = 16.8436(2) Å, β = 112.0657(4)°, V = 3092.36(5) Å^3, Z = 4, D_{calc} = 1.503 g cm^{-3}, F(000) = 1416, μ = 4.665 mm^{-1}. Preliminary examination and data collection were carried out on a κ-CCD device (Nonius, Mach3) with an Oxford Cryosystems cooling system at the window of a rotating anode (Nonius FR591) with graphite-monochromated Mo-K_α radiation (λ = 0.71073 Å). Data collection was performed at 173 K within the Θ range 1.43° < Θ < 23.35°. A total of 37465 intensities were integrated. Raw data were corrected for Lorentz, polarization, and latent decay and absorption effects arising from the scaling procedure. After merging (R_{int} = 0.0167), 5676 [5124: $I_0 > 2\sigma(I_0)$] independent reflections remained and all were used to refine 322 parameters. The structure was solved by a combination of direct methods and difference-Fourier syntheses. All non-hydrogen atoms were refined with anisotropic displacement parameters. All hydrogen atoms were placed in calculated positions and refined using a riding model. Full-matrix least-squares refinements were carried out by minimizing $\Sigma w(F_o^2 - F_c^2)^2$ and converged with $R1$ = 0.0204 [$I_0 > 2\sigma(I_0)$], $wR2$ = 0.0451 (all data), GOF = 1.061, and shift/error < 0.001. The final difference-Fourier map showed no striking features ($\Delta e_{min/max}$ = +0.82/–1.14 e Å^{-3}). CCDC-613908.

***cis*-[1′]Pt(*n*Pr)$_2$:** White powder, yield: 64%. ^1H NMR ([D$_8$]toluene): δ = 0.63 (br. t, $^3J_{H,H}$ = 7.4 Hz, 6 H, CH_3), 0.97 (m, 4 H, CH_2CH$_3$), 1.18 (m, 4 H, PtCH_2), 6.69 (d, $^3J_{H,H}$ = 7.4 Hz, 2 H, biphenyl-CH), 6.83 (d, $^3J_{H,H}$ = 7.4 Hz, 2 H, biphenyl-CH), 6.89 (t, $^3J_{H,H}$ = 7.4 Hz, 2 H, biphenyl-CH), 7.12 (t, $^3J_{H,H}$ = 7.4 Hz, 6 H, CH arom.), 7.24-7.33 (m, 16 H, CH-arom.) ppm. $^{13}C\{^1H\}$ NMR ([D$_8$]toluene): δ = 4.6 (br. s, CH_3), 15.6 (s, $^3J_{C,P}$ = 2.9, $^2J_{C,Pt}$ = 41.7 Hz, *C*H$_2$CH$_3$), 23.9 (m pseudo t, $^1J_{C,Pt}$ = 501.3 Hz, PtCH$_2$), 130.9 (s), 131.1 (s), 131.2 (s), 131.3 (s), 131.3 (s), 131.4 (s), 131.7 (s), 131.8 (s), 131.9 (s), 132.0 (s), 132.3 (s), 132.3 (s), 132.6 (s), 132.7 (s), 132.8 (s), 133.5 (s), 140.7 (br. s), 153.3 (pseudo t, $^3J_{C,P}$ = 4.4 Hz, COP) ppm. $^{31}P\{^1H\}$ NMR ([D$_8$]toluene): δ = 111.8 (pseudo t, $^1J_{P,Pt}$ = 1970.5 Hz) ppm. $^{195}Pt\{^1H\}$ NMR ([D$_8$]toluene): δ = –4526.1 (t, $^1J_{P,Pt}$ = 1970.5 Hz) ppm.

General Synthetic Procedure for the *trans*-[Ligand*]^{X}PtCl$_2$ Complexes: *trans*-Dichlorido(η^2-ethylene)(pyridine)platinum(II) (0.27 mmol) and ligand (0.54 mmol) were dissolved in 10 mL of dichloromethane and stirred overnight at room temperature. After removing the solvent in vacuo the residue was washed with diethyl ether and dried in vacuo.

***trans*-[1*]^{I}PtCl$_2$:** Light-yellow powder. Yield: 92%. ^1H NMR ($CDCl_3$): δ = 1.35 (d, $^3J_{H,H}$ = 7.8 Hz, 3 H, CHCH_3), 1.37 (d, $^3J_{H,H}$ = 8.8 Hz, 6 H, CHCH_3), 1.39 (d, $^3J_{H,H}$ = 7.8 Hz, 6 H, CHCH_3), 1.41 (d, $^3J_{H,H}$ = 8.1 Hz, 6 H, CHCH_3), 1.43 (d, $^3J_{H,H}$ = 7.6 Hz, 3 H, CHCH_3), 2.92–3.01 (m, 4 H, C*H*CH$_3$), 6.74–6.78 (m, 2 H, CH arom.), 7.20–7.24 (m, 2 H, CH arom.), 7.70 (m, 2 H, CH arom.), 7.89 (d, $^3J_{H,H}$ = 8.1 Hz, 2 H, CH arom.) ppm. $^{13}C\{^1H\}$ NMR ($CDCl_3$): δ = 17.5 (s, CH*C*H$_3$), 18.3 (s, CH*C*H$_3$), 28.3 (pseudo t, $^1J_{C,P}$ = 16.8 Hz, *C*HCH$_3$), 89.0 (s, C–I), 120.1 (s, CH arom.), 124.8 (s, CH arom.), 128.7 (s, CH arom.), 139.6 (s, CH arom.), 154.4 (s, CH arom.) ppm. $^{31}P\{^1H\}$ NMR ($CDCl_3$): δ = 128.3 (s, $^1J_{P,Pt}$ = 2631.6 Hz) ppm. $^{195}Pt\{^1H\}$ NMR ($CDCl_3$): δ = –3796.8 (t, $^1J_{P,Pt}$ = 2631.6 Hz) ppm. $C_{24}H_{36}Cl_2I_2O_2P_2Pt$ (938.27): calcd. C 30.72, H 3.87, Cl 7.56, P 6.60; found C 30.85, H 3.95, Cl 7.92, P 6.62.

Crystal-Structure Analysis of *trans*-[1*]^{I}PtCl$_2$: $C_{24}H_{36}Cl_2I_2O_2P_2Pt$, M_r = 938.27, colorless needle (0.11 × 0.12 × 0.19 mm^3), monoclinic, $P2_1/n$ (no. 14), a = 8.0215(1), b = 12.6774(2), c = 16.6598(3) Å, β = 94.9889(7)°, V = 1687.8(18) Å^3, Z = 4, D_{calc} = 3.692 g cm^{-3}, F(000) = 1776, μ = 12.513 mm^{-1}. Preliminary examination and data collection were carried out on a κ-CCD device (Nonius, Mach3) with an Oxford Cryosystems cooling system at the window of a rotating anode (Nonius FR591) with graphite-monochromated Mo-K_α radiation (λ = 0.71073 Å). Data collection was performed at 173 K within the Θ range 2.02° < Θ < 25.34°. A total of 14416 intensities were integrated. Raw data were corrected for Lorentz, polarization, and latent decay and absorption effects arising from the scaling procedure. After merging (R_{int} = 0.0216), 3086 [2611: $I_0 > 2\sigma(I_0)$] independent reflections remained and all were used to refine 165 parameters. The structure was solved by a combination of direct methods and difference-Fourier syntheses. All non-hydrogen atoms were refined with anisotropic displacement parameters. All hydrogen atoms were placed in calculated positions and refined using a riding model. Full-matrix least-squares refinements were carried out by minimizing $\Sigma w(F_o^2 - F_c^2)^2$ and converged with $R1$ = 0.0279 [$I_0 > 2\sigma(I_0)$], $wR2$ = 0.0793 (all data), GOF = 1.077, and shift/error < 0.001. The final difference-Fourier map showed no striking features ($\Delta e_{min/max}$ = +1.09/–0.97 e Å^{-3}). CCDC-613910.

***trans*-[3*]^{I}PtCl$_2$:** Light-yellow powder, yield: 90%. *trans*-Dichlorido(η^2-ethylene)(pyridine)platinum(II) (0.1 g, 0.27 mmol) and (2-iodobenzoxy)diisopropylphosphane (0.18 g, 0.54 mmol) were dissolved in 10 mL of dichloromethane and stirred overnight at room temperature. After stripping off the solvent in vacuo the residue was washed with 3 mL of diethyl ether and dried in vacuo. Yellow powder: 0.24 g (90%). ^1H NMR ($CDCl_3$): δ = 1.33 (d, $^3J_{H,H}$ = 7.4 Hz, 3 H, CHCH_3), 1.37 (d, $^3J_{H,H}$ = 7.4 Hz, 6 H, CHCH_3), 1.41 (d, $^3J_{H,H}$ = 8.6 Hz, 6 H, CHCH_3), 1.45 (d, $^3J_{H,H}$ = 8.6 Hz, 6 H, CHCH_3), 2.67–2.73 (m, 4 H, C*H*CH$_3$), 5.26 (m, 4 H, CH arom.), 6.96 (m, 2 H, CH arom.), 7.32 (t, $^3J_{H,H}$ = 7.4 Hz, 2 H, CH arom.), 7.60 (d, $^3J_{H,H}$ = 7.4 Hz, 2 H, CH arom.), 7.76 (d, $^3J_{H,H}$ = 7.4 Hz, 2 H, CH arom.) ppm. $^{13}C\{^1H\}$ NMR ($CDCl_3$): δ = 16.7 (s, CH*C*H$_3$), 17.9 (s, CH*C*H$_3$), 26.9 (d, $^1J_{C,P}$ = 17.6 Hz, *C*HCH$_3$), 27.2 (d, $^1J_{C,P}$ = 18.3 Hz, *C*HCH$_3$), 74.8 (s, CH$_2$), 96.7 (s, C–I), 128.2 (s, CH arom.), 128.5 (s, CH arom.), 129.2 (s, CH arom.), 138.8 (s, CH arom.), 140.4 (d, $J_{C,P}$ = 3.7 Hz, CH$_2$*C*), 140.5 (d, $J_{C,P}$ = 4.4 Hz, CH$_2$*C*) ppm. $^{31}P\{^1H\}$ NMR ($CDCl_3$): δ = 129.9 (pseudo t, $^1J_{P,Pt}$ = 2603.7 Hz) ppm. $^{195}Pt\{^1H\}$ NMR ($CDCl_3$): δ = –3758.9 (t, $^1J_{P,Pt}$ = 2603.7 Hz) ppm. $C_{26}H_{40}Cl_2I_2O_2P_2Pt$ (966.32): calcd. C 32.31, H 4.17, P 6.61; found C 32.24, H 4.06, P 6.14.

General Synthetic Procedure for the *cis*-[Ligand*]^{X}PtCl$_2$ Complexes: [(COD)PtCl$_2$] 0.27 mmol and ligand 0.54 mmol were dissolved in 10 mL of dichloromethane and stirred overnight at room temperature. After removing the solvent in vacuo the residue was washed with diethyl ether and dried in vacuo.

***cis*-[1*]^{Br}PtCl$_2$:** Off-white powder. Yield: 97%. ^1H NMR ($CDCl_3$): δ = 1.37 (dd, $^3J_{H,H}$ = 7.4, $^3J_{P,H}$ = 6.1 Hz, 12 H, CHCH_3), 1.55 (d, $^3J_{H,H}$ = 7.4, $^3J_{P,H}$ = 6.1 Hz, 12 H, CHCH_3), 3.20 (dsept, $^3J_{H,H}$ = 7.4, $^1J_{P,H}$ = 6.1 Hz, 4 H, C*H*CH$_3$), 6.85 (t, $^3J_{H,H}$ = 7.4 Hz, 2 H, CH arom.), 7.07 (t, $^3J_{H,H}$ = 7.4 Hz, 2 H, CH arom.), 7.24 (d, $^3J_{H,H}$ = 7.4 Hz, 2 H, CH arom.), 7.38 (d, $^3J_{H,H}$ = 7.4 Hz, 2 H, CH arom.) ppm. $^{13}C\{^1H\}$ NMR ($CDCl_3$): δ = 18.2 (s, CH*C*H$_3$), 19.6 (s, CH*C*H$_3$), 31.3 (d, $^1J_{C,P}$ = 33.7 Hz, *C*HCH$_3$), 113.9 (s, CH arom.), 120.2 (s, CH arom.), 124.8 (s, CH arom.), 128.1 (s, CH arom.), 134.0 (s, CH arom.), 149.7 (d, $^2J_{C,P}$ = 13.2 Hz, CH arom.) ppm. $^{31}P\{^1H\}$ NMR ($CDCl_3$): δ = 124.3 (br. pseudo t, $^1J_{P,Pt}$ = 4191.1 Hz) ppm. $^{195}Pt\{^1H\}$ NMR ($CDCl_3$): δ = –4299.7 (t, $^1J_{P,Pt}$ = 4191.4 Hz) ppm. $C_{24}H_{36}Br_2Cl_2O_2P_2Pt$ (844.28): calcd. C 34.14, H 4.30; found C 34.07, H 4.33.

Crystal-Structure Analysis of *cis*-[1*]^{Br}PtCl$_2$·(CH$_2$Cl$_2$): $C_{25}H_{38}Br_2Cl_4O_2P_2Pt$, M_r = 1014.13, colorless needle ($0.10 \times 0.15 \times 0.22$ mm^3), monoclinic, $C2/c$ (no. 15), a = 18.2485(9), b = 14.6811(9), c = 15.6006(9) Å, β = 119.725(2)°, V = 3629.6(4) Å^3, Z = 4, D_{calc} = 1.856 g cm^{-3}, $F(000)$ = 1968, μ = 6.621 mm^{-1}. Preliminary examination and data collection were carried out on a κ-CCD device (Nonius, Mach3) with an Oxford Cryosystems cooling system at the window of a rotating anode (Nonius FR591) with graphite-monochromated Mo-K_α radiation (λ = 0.71073 Å). Data collection was performed at 173 K within the Θ range 1.89° < Θ < 25.38°. A total of 17358 intensities were integrated. Raw data were corrected for Lorentz, polarization, and latent decay and absorption effects arising from the scaling procedure. After merging (R_{int} = 0.061), 1891 [1551: $I_0 > 2\sigma(I_0)$] independent reflections remained and all were used to refine 175 parameters. The structure was solved by a combination of direct methods and difference-Fourier syntheses. All non-hydrogen atoms were refined with anisotropic displacement parameters. All hydrogen atoms were placed in calculated positions and refined using a riding model. Full-matrix least-squares refinements were carried out by minimizing $\Sigma w(F_o^2 - F_c^2)^2$ and converged with $R1$ = 0.0751 [$I_0 > 2\sigma(I_0)$], $wR2$ = 0.1761 (all data), GOF = 1.106, and shift/error < 0.001 ($\Delta e_{min/max}$ = +1.98/–1.54 e Å^{-3}). CCDC-613911.

***cis*-[3*]^{Br}PtCl$_2$:** Off-white powder. Yield: 89%. ^{1}H NMR ($CDCl_3$): δ = 1.33 (dd, $^3J_{H,H}$ = 7.4, $^3J_{P,H}$ = 6.1 Hz, 12 H, CHCH_3), 1.57 (d, $^3J_{H,H}$ = 7.4, $^3J_{P,H}$ = 6.1 Hz, 12 H, CHCH_3), 3.05 (dsept, $^3J_{H,H}$ = 7.4, $^1J_{P,H}$ = 6.1 Hz, 4 H, CHCH$_3$), 4.76 (d, $^3J_{P,H}$ = 4.9 Hz, 4 H, O-CH_2), 7.04 (t, $^3J_{H,H}$ = 7.4 Hz, 2 H, CH arom.), 7.14 (t, $^3J_{H,H}$ = 7.4 Hz, 2 H, CH arom.), 7.29 (d, $^3J_{H,H}$ = 7.4 Hz, 2 H, CH arom.), 7.36 (d, $^3J_{H,H}$ = 7.4 Hz, 2 H, CH arom.) ppm. ^{13}C{^{1}H} NMR ($CDCl_3$): δ = 18.2 (s, CHCH$_3$), 19.6 (s, CHCH$_3$), 29.6 (d, $^1J_{C,P}$ = 4.0 Hz, CHCH$_3$), 68.8 (d, $^2J_{C,P}$ = 11.0 Hz, CH_2), 121.0 (s, CH arom.), 127.2 (s, CH arom.), 127.4 (s, CH arom.), 129.3 (s, CH arom.), 132.5 (s, CH arom.), 135.1 (s, CH arom.) ppm. ^{31}P{^{1}H} NMR ($CDCl_3$): δ = 123.1 (s, $^1J_{P,Pt}$ = 4191.4 Hz) ppm. ^{195}Pt{^{1}H} NMR ($CDCl_3$): δ = –4299.7 (t, $^1J_{P,Pt}$ = 4191.4 Hz) ppm. $C_{26}H_{40}Br_2Cl_2O_2P_2Pt$ (872.33): calcd. C 35.80, H 4.62; found C 35.70, H 4.71.

General Synthetic Procedure for the [Ligand*]Pt Complexes: The complex (ligand)^{X}PtCl$_2$ (0.27 mol) was dissolved in 20 mL of toluene and the solution was cooled with dry ice. Then 0.54 mol of *s*BuLi (1.3 M solution in benzene/hexane) was added with a syringe and the solution was stirred overnight while warming up to room temperature. The next day it was filtered and the solvent removed in vacuo. The remaining white solid was washed with three 5-mL portions of pentane and dried in vacuo.

***cis*-[1*]Pt:** White powder, yield: 85%. ^{1}H NMR ($CDCl_3$): δ = 1.10 (d, $^3J_{H,H}$ = 6.84 Hz, 6 H, CHCH_3), 1.15 (d, $^3J_{H,H}$ = 7.8 Hz, 6 H, CHCH_3), 1.19 (d, $^3J_{H,H}$ = 6.84 Hz, 6 H, CHCH_3), 1.22 (d, $^3J_{H,H}$ = 6.84 Hz, 6 H, CHCH_3), 2.36 (m, 4 H, CHCH$_3$), 6.91 (m, 2 H, CH arom.), 6.99–7.07 (m, 4 H, CH arom.), 7.74 (t, $^3J_{H,H}$ = 6.3, $J_{H,Pt}$ = 47.0 Hz, 2 H, CH arom.) ppm. ^{13}C{^{1}H} NMR (C_7D_8): δ = 16.8 (pseudo t, $J_{C,Pt}$ = 15.4 Hz, P-CH-CH$_3$), 17.8 (m, P-CH-CH$_3$), 30.8 (d pseudo t, $^1J_{C,P}$ = 22.0, $^2J_{C,Pt}$ = 21.2 Hz, P-CH), 110.2 (d pseudo t, $^3J_{C,P}$ = 13.2, $^2J_{C,Pt}$ = 6.6 Hz, *C*-arom.), 122.4 (pseudo t, $^3J_{C,Pt}$ = 53.4 Hz, *C*-arom.), 126.6 (s, *C*-arom.), 141.2 (pseudo t, $^3J_{C,Pt}$ = 38.1 Hz, *C*-arom.), 150.0 (d pseudo t, $^1J_{C,Pt}$ = 850.4, $^2J_{C,P}$*cis* = 9.0, $^2J_{C,P}$*trans* = 104.7 Hz, *C*-Pt), 167.6 (d pseudo t, $^2J_{C,P}$ = 8.8, $^2J_{C,Pt}$ = 8.8 Hz, O-*C*) ppm. ^{31}P{^{1}H} NMR ($CDCl_3$): δ = 179.0 (pseudo t, $^1J_{P,Pt}$ = 2147.2 Hz) ppm. ^{195}Pt{^{1}H} NMR ($CDCl_3$): δ = –4583.9 (t, $^1J_{P,Pt}$ = 2147.2 Hz) ppm. MS (FAB): *m*/*z* (%) 613.1 (100) [M], with correct isotope pattern for $C_{24}H_{36}O_2P_2Pt$. $C_{24}H_{36}O_2P_2Pt$ (613.57): calcd. C 46.98, H 5.91; found C 46.76, H 5.82.

Crystal-Structure Analysis of *cis*-[1*]Pt: $C_{24}H_{36}O_2P_2Pt$, M_r = 613.56, colorless fragment ($0.11 \times 0.14 \times 0.20$ mm^3), monoclinic, $P2_1/n$ (no. 14), a = 12.5818(1), b = 13.8769(1), c = 15.2961(1) Å, β = 106.9606(4)°, V = 2554.49(3) Å^3, Z = 4, D_{calc} = 1.595 g cm^{-3}, $F(000)$ = 1216, μ = 5.635 mm^{-1}. Preliminary examination and data collection were carried out on a κ-CCD device (Nonius, Mach3) with an Oxford Cryosystems cooling system at the window of a rotating anode (Nonius FR591) with graphite-monochromated Mo-K_α radiation (λ = 0.71073 Å). Data collection was performed at 173 K within the Θ range 1.85° < Θ < 25.35°. A total of 55295 intensities were integrated. Raw data were corrected for Lorentz, polarization, and latent decay and absorption effects arising from the scaling procedure. After merging (R_{int} = 0.0789), 4739 [3137: $I_0 > 2\sigma(I_0)$] independent reflections remained and all were used to refine 270 parameters. The structure was solved by a combination of direct methods and difference-Fourier syntheses. All non-hydrogen atoms were refined with anisotropic displacement parameters. All hydrogen atoms were placed in calculated positions and refined using a riding model. Full-matrix least-squares refinements were carried out by minimizing $\Sigma w(F_o^2 - F_c^2)^2$ and converged with $R1$ = 0.0399 [$I_0 > 2\sigma(I_0)$], $wR2$ = 0.0709 (all data), GOF = 0.997, and shift/error < 0.001. The final difference-Fourier map showed no striking features ($\Delta e_{min/max}$ = +1.43/–1.16 e Å^{-3}). CCDC-613903.

***cis*-[3*]Pt:** White powder, yield: 91%. ^{1}H NMR (C_7D_8, –80 °C): δ = 0.59 (dd, $^3J_{H,H}$ = 7.36, $^3J_{P,H}$ = 6.12 Hz, 3 H, CH_3), 0.79 (dd, $^3J_{H,H}$ = 7.36, $^3J_{P,H}$ = 11.00 Hz, 3 H, CH_3), 1.07 (dd, $^3J_{H,H}$ = 9.80, $^3J_{P,H}$ = 6.16 Hz, 3 H, CH_3), 1.60 (dsept, $^3J_{H,H}$ = 7.36, $^2J_{P,H}$ = 7.36 Hz, 2 H, P-CH), 1.80 (dsept, $^3J_{H,H}$ = 7.36, $^2J_{P,H}$ = 4.88 Hz, 2 H, P-CH), 4.62 (dd, $^2J_{H,H}$ = 9.8, $^4J_{P,H}$ = 27.59 Hz, 2 H, CHH-O), 5.04 (dd, $^2J_{H,H}$ = 9.8, $^4J_{P,H}$ = 10.42 Hz, 2 H, CHH-O), 7.31 (m, 2 H, arom. CH), 7.38 (m, 2 H, arom. CH), 8.04 (d, $^3J_{H,H}$ = 7.36 Hz, 2 H, arom. CH) ppm. ^{13}C{^{1}H} NMR ($CDCl_3$): δ = 17.1 (br. s, CH$_3$), 18.9 (d pseudo t, $^2J_{C,P}$ = 5.6, $^3J_{C,Pt}$ = 5.4 Hz, CH$_3$), 31.7 (m, P-CH), 79.1 (pseudo t, $^3J_{C,Pt}$ = 101.0 Hz, CH$_2$-O), 122.6 (pseudo t, $J_{C,Pt}$ = 5.0 Hz, *C*-arom.), 125.4 (d pseudo t, $J_{C,P}$ = 5.1, $J_{C,Pt}$ = 34.4 Hz, *C*-arom.), 126.8 (d pseudo t, $J_{C,P}$ = 5.1, $J_{C,Pt}$ = 64.4 Hz, *C*-arom.), 140.4 (m, C-arom.), 140.7 (pseudo t, $J_{C,Pt}$ = 39.5 Hz, C-arom.), 158.2 (d pseudo t, $^1J_{C,Pt}$ = 808.0, $^2J_{C,P}$*cis* = 13.2, $^2J_{C,P}$*trans* = 103.2 Hz, *C*-Pt) ppm. ^{31}P{^{1}H} NMR ($CDCl_3$): δ = 128.5 (pseudo t, $^1J_{P,Pt}$ = 2072.9 Hz) ppm. ^{195}Pt{^{1}H} NMR ($CDCl_3$): δ = –4644.3 (t, $^1J_{P,Pt}$ = 2072.9 Hz) ppm. MS (FAB): *m*/*z* (%) 642.1 (100) [M], with correct isotope pattern for $C_{26}H_{40}O_2P_2Pt$.

Crystal-Structure Analysis of *cis*-[3*]Pt: $C_{26}H_{40}O_2P_2Pt$, M_r = 712.53, colorless fragment ($0.05 \times 0.11 \times 0.21$ mm^3), monoclinic, $P2_1/n$ (no. 14), a = 8.8313(1), b = 25.0326(3), c = 14.2562(2) Å, β = 104.8610(6)°, V = 3046.20(7) Å^3, Z = 4, D_{calc} = 1.399 g cm^{-3}, $F(000)$ = 1280, μ = 4.728 mm^{-1}. Preliminary examination and data collection were carried out on a κ-CCD device (Nonius, Mach3) with an Oxford Cryosystems cooling system at the window of a rotating anode (Nonius FR591) with graphite-monochromated Mo-K_α radiation (λ = 0.71073 Å). Data collection was performed at 215 K within the Θ range 1.63° < Θ < 25.36°. A total of 64277 intensities were integrated. Raw data were corrected for Lorentz, polarization, and latent decay and absorption effects arising from the scaling procedure. After merging (R_{int} = 0.0338), 3716 [3069: $I_0 > 2\sigma(I_0)$] independent reflections remained and all were used to refine 288 parameters. The structure was solved by a combination of direct methods and difference-Fourier syntheses. All non-hydrogen atoms were refined with anisotropic displacement parameters. All hydrogen atoms were placed in calculated positions and refined using a riding model. Full-matrix least-squares refinements were carried out by minimizing $\Sigma w(F_o^2 - F_c^2)^2$ and converged with $R1$ = 0.0361 [$I_0 > 2\sigma(I_0)$], $wR2$ = 0.0867 (all data), GOF = 1.053, and

shift/error < 0.001. The final difference-Fourier map showed no striking features ($\Delta e_{min/max}$ = +0.79/–0.61 e Å^{-3}). CCDC-613905.

***trans*-[1*]Pt:** White powder, yield: 87%. ^{1}H NMR (C_7D_8): δ = 1.08 (dd, $^3J_{H,H}$ = 7.32, $^3J_{P,H}$ = 7.32 Hz, 12 H, C*H*$_3$), 1.12 (dd, $^3J_{H,H}$ = 8.80, $^3J_{P,H}$ = 8.80 Hz, 12 H, C*H*$_3$), 2.28 (sept, $^3J_{H,H}$ = 7.32 Hz, 4 H, C*H*CH$_3$), 6.87 (t, $^3J_{H,H}$ = 7.28 Hz, 2 H, arom. CH), 7.08 (t, $^3J_{H,H}$ = 7.32 Hz, 2 H, arom. CH), 7.28 (d, $^3J_{H,H}$ = 7.32 Hz, 2 H, arom. CH), 7.81 (d pseudo t, $^3J_{H,H}$ = 7.32, $^3J_{Pt,H}$ = 39.5 Hz, 2 H, arom. CH) ppm. ^{13}C{^{1}H} NMR (C_7D_8): δ = 16.7 (br. s, *C*H$_3$), 18.2 (br. s, *C*H$_3$), 29.51 (pseudo t, $^1J_{C,P}$ = 35.85 Hz, P-*C*H), 111.3 (pseudo t, $^2J_{C,Pt}$ = 11.96 Hz), 121.8 (pseudo t, $^3J_{C,Pt}$ = 37.69 Hz), 125.9 (s), 143.6 (pseudo t, $^2J_{C,Pt}$ = 9.20 Hz, C-O), 168.4 (dd, $^2J_{C,P\,cis\,A}$ = 6.42, $^2J_{C,P\,cis\,B}$ = 7.35 Hz, C-Pt) ppm. ^{31}P{^{1}H} NMR (C_7D_8): δ = 173.7 (pseudo t, $^1J_{P,Pt}$ = 2998.6 Hz) ppm. ^{195}Pt{^{1}H} NMR (C_7D_8): δ = –4349.7 (pseudo t, $^1J_{P,Pt}$ = 2998.6 Hz) ppm. MS (FAB): *m*/*z* (%) 613.1 (100) [M], with correct isotope pattern for $C_{24}H_{36}O_2P_2Pt$.

Crystal-Structure Analysis of *trans*-[1*]Pt: $C_{24}H_{36}O_2P_2Pt$, M_r = 613.56, colorless needle (0.09 × 0.12 × 0.25 mm^3), monoclinic, $P2_1/c$ (no. 14), a = 7.8126(1), b = 16.4322(3), c = 9.9638(2) Å, β = 109.5947(8)°, V = 1205.1(3) Å^3, Z = 4, D_{calc} = 3.382 g cm^{-3}, F(000) = 1216, μ = 11.943 mm^{-1}. Preliminary examination and data collection were carried out on a κ-CCD device (Nonius, Mach3) with an Oxford Cryosystems cooling system at the window of a rotating anode (Nonius FR591) with graphite-monochromated Mo-K_α radiation (λ = 0.71073 Å). Data collection was performed at 173 K within the Θ range 2.48° < Θ < 25.32°. A total of 11134 intensities were integrated. Raw data were corrected for Lorentz, polarization, and latent decay and absorption effects arising from the scaling procedure. After merging (R_{int} = 0.0244), 2196 [1894: $I_0 > 2\sigma(I_0)$] independent reflections remained and all were used to refine 138 parameters. The structure was solved by a combination of direct methods and difference-Fourier syntheses. All non-hydrogen atoms were refined with anisotropic displacement parameters. All hydrogen atoms were placed in calculated positions and refined using a riding model. Full-matrix least-squares refinements were carried out by minimizing $\Sigma w(F_o^2 - F_c^2)^2$ and converged with $R1$ = 0.0171 [$I_0 > 2\sigma(I_0)$], $wR2$ = 0.0412 (all data), GOF = 1.052, and shift/error < 0.001. The final difference-Fourier map showed no striking features ($\Delta e_{min/max}$ = +0.88/–0.76 e Å^{-3}). CCDC-613909.

[3]Pt: Off-white powder, yield: quantitative. ^{1}H NMR (C_7D_8): δ = –17 (t pseudo t, $^2J_{P,H}$ = 4.9 Hz $^1J_{Pt,H}$ = 1208.1 Hz, 0.7 H, agost. H), 0.95 (dd, $^3J_{H,H}$ = 7.4 Hz $^3J_{H,P}$ = 7.4 Hz, 6 H, CH$_3$), 1.10 (dd, $^3J_{H,H}$ = 7.4 Hz $^3J_{H,P}$ = 7.4 Hz, 6 H, CH$_3$), 1.16 (dd, $^3J_{H,H}$ = 7.3 Hz $^3J_{H,P}$ = 7.4 Hz, 6 H, CH$_3$), 1.26 (dd, $^3J_{H,H}$ = 7.4, $^3J_{H,P}$ = 9.8 Hz, 6 H, CH$_3$), 2.35 (hept., $^3J_{H,H}$ = 7.4 Hz, 2 H, C*H*-CH$_3$), 2.43 (hept., $^3J_{H,H}$ = 7.4 Hz, 2 H, C*H*-CH$_3$), 4.61 (dd, $^2J_{H,H}$ = 9.8 Hz $^3J_{P,H}$ = 12.24 Hz, 2 H, CH$_2$-O), 4.90 (dd, $^2J_{H,H}$ = 7.4 Hz $^3J_{P,H}$ = 7.4 Hz, 2 H, CH$_2$-O), 6.66 (d, $^3J_{H,H}$ = 7.4 Hz, 2 H, CH arom.), 6.95 (t, $^3J_{H,H}$ = 7.4 Hz, 2 H, CH arom.), 7.18 (t, $^3J_{H,H}$ = 7.4 Hz, 2 H, CH arom.), 7.61 (d, $^3J_{H,H}$ = 7.4 Hz, 2 H, CH arom.) ppm. ^{13}C{^{1}H} NMR ($CDCl_3$): δ = 16.65 (pseudo t, $J_{C,Pt}$ = 21.9 Hz), 17.3–17.6 (several br. s, CH$_3$), 27.70 (t, $^1J_{P,C}$ = 20.1 Hz, *C*HCH$_3$), 29.50 (t, $^1J_{P,C}$ = 16.5 Hz, *C*HCH$_3$), 70.52 (pseudo t, $^3J_{C,Pt}$ = 83.1 Hz, CH$_2$), 122.89 (s, arom. C), 126.55 (s, arom. C), 130.14 (s, arom. C), 136.87 (s, arom. C), 138.49 (s, arom. C) ppm. ^{31}P{^{1}H} NMR (C_7D_8): δ = 160.1 (pseudo t, $^1J_{P,Pt}$ = 3158.8 Hz) ppm. ^{195}Pt{^{1}H} NMR (C_7D_8): δ = –4894.8 (t, $^1J_{P,Pt}$ = 3158.8 Hz) ppm. MS (FAB): *m*/*z* 642.3 [M + 1], with correct isotopic pattern. FT-IR (KBr): $\tilde{\nu}$ = 1945 cm^{-1} (w, Pt–H).

Calculations: The DFT calculations were performed using the program suite Gaussian 03.[5] All molecular geometries were fully optimized. The DFT method used includes Becke's three parameter hybrid exchange functional in combination with the correlation functional of Perdew and Wang (B3PW91). Geometry optimizations and frequency calculations were performed using the valence double-zeta LANL2DZ basis set. The frozen-coordinate analysis was done using the program codes implemented in Gaussian 03.

Single Crystal X-ray Structure Determination of Compounds *cis*-[2]PtCl$_2$·2(CHCl$_3$), *trans*-[2]PtCl$_2$, *cis*-[3]PtCl$_2$·3(CHCl$_3$), *trans*-[3]PtCl$_2$, *cis*-[1]Pt(*n*Pr)$_2$, *cis*-[3]PtEt$_2$, *trans*-[1*]^{1}PtCl$_2$, *cis*-[1*]^{Br}PtCl$_2$·(CH$_2$Cl$_2$), *trans*-[1*]Pt, *cis*-[1*]Pt, and *cis*-[3*]Pt: The crystal was stored under perfluorinated ether, transferred into a Lindemann capillary, fixed, and sealed. Preliminary examination and data collection were carried out as described above for each complex. Neutral atom scattering factors for all atoms and anomalous dispersion corrections for the non-hydrogen atoms were taken from the International Tables for Crystallography.[12d] All calculations were performed on an Intel Pentium II PC, with the STRUX-V system, including the programs PLATON, SIR92, and SHELXL-97.[12]

CCDC-613903 to -613913 contain the supplementary crystallographic data for this paper. These data can be obtained free of charge from The Cambridge Crystallographic Data Centre via www.ccdc.cam.ac.uk/data_request/cif.

Acknowledgments

K. R. thanks the Deutsche Forschungsgemeinschaft (DFG) for financial support (Ru519/3-2) and the Fonds der Chemischen Industrie for a Liebig grant. He is also grateful to Prof. Dr. mult. W. A. Herrmann for financial support.

[1] a) B. L. Edelbach, R. J. Lachicotte, W. D. Jones, *J. Am. Chem. Soc.* **1998**, *120*, 2843–2853; b) G. Ujaque, F. Maseras, O. Eisenstein, L. Liable-Sands, A. L. Rheingold, W. Yao, R. H. Crabtree, *New J. Chem.* **1998**, *22*, 1493–1498; c) Z. Lu, C. H. Jun, S. R. de Gala, M. P. Sigalas, O. Eisenstein, R. H. Crabtree, *Organometallics* **1995**, *14*, 1168–1175; d) C. N. Iverson, W. D. Jones, *Organometallics* **2001**, *20*, 5745–5750; e) X. Zhang, G. B. Carpenter, D. A. Sweigart, *Organometallics* **1999**, *18*, 4887–4888; f) H. Schwager, S. Spyroudis, K. P. C. Vollhardt, *J. Organomet. Chem.* **1990**, *382*, 191–200; g) J. J. Eisch, A. M. Piotrowski, K. I. Han, C. Krüger, Y. H. Tsay, *Organometallics* **1985**, *4*, 224–231; h) R. M. Shaltout, R. Sygula, A. Sygula, F. R. Fronczek, G. G. Stanley, P. W. Rabideau, *J. Am. Chem. Soc.* **1998**, *120*, 835–836; i) T. Schaub, U. Radius, *Chem. Eur. J.* **2005**, *11*, 5024–5030.

[2] a) A. E. Shilov, G. B. Shul'pin, *Chem. Rev.* **1997**, *97*, 2879–2932; b) R. H. Crabtree, *Chem. Rev.* **1985**, *85*, 245–269; c) J. Halpern, *Inorg. Chim. Acta* **1985**, *100*, 41–48; d) G. W. Parshall, *Acc. Chem. Res.* **1975**, *8*, 113–117; e) *Activation and Catalytic Reactions of Saturated Hydrocarbons in the Presence of Metal Complexes* (Eds.: A. E. Shilov, G. B. Shul'pin), Kluwer Academic Publishers **2000**, Dordrecht, The Netherlands; f) *Selective Hydrocarbon Activation* (Eds.: J. A. Davies, P. L. Watson, J. F. Liebman, A. Greenberg), VCH Publishers, New York/Weinheim, **1990**; g) *Theoretical Aspects of Homogeneous Catalysis* (Eds.: P. W. N. M. van Leeuwen, K. Morokuma, J. H. van Lenthe), Kluwer Academic Publishers, Dordrecht, The Netherlands, **1995**; h) A. D. Ryabov, *Chem. Rev.* **1990**, *90*, 403–424; i) W. D. Jones, F. J. Feher, *Acc. Chem. Res.* **1989**, *22*, 91–100; j) B. A. Arndtsen, R. G. Bergman, T. A. Mobley, T. H. Peterson, *Acc. Chem. Res.* **1995**, *28*, 154–162; k) B. Rybtchinski, D. Milstein, *Angew. Chem. Int. Ed.* **1999**, *38*, 870–883; l) C.-H. Jun, *Chem. Soc. Rev.* **2004**, *33*, 610–618.

[3] K. Ruhland, E. Herdtweck, *J. Organomet. Chem.* **2005**, *690*, 5215–5236.

[4] a) J. W. Suggs, C.-H. Jun, *J. Am. Chem. Soc.* **1984**, *106*, 3054; b) J. W. Suggs, C.-H. Jun, *J. Am. Chem. Soc.* **1986**, *108*, 4679; c) J. W. Suggs, C.-H. Jun, *J. Chem. Soc., Chem. Commun.* **1985**, 92; d) N. Chatani, Y. Ie, F. Kakiuchi, S. Murai, *J. Am. Chem. Soc.* **1999**, *121*, 8645; e) S.-Y. Liou, M. E. van der Boom, D. Milstein, *Chem. Commun.* **1998**, 687; f) B. Rybtchinski, S. Oevers, M. Montag, A. Vigalok, H. Rozenberg, J. M. L. Martin, D. Milstein, *J. Am. Chem. Soc.* **2001**, *123*, 9064–9077; g) A. Sundermann, O. Uzan, D. Milstein, J. M. L. Martin, *J. Am. Chem. Soc.* **2000**, *122*, 7095–7104; h) B. Rybtchinski, D. Milstein, *J. Am. Chem. Soc.* **1999**, *121*, 4528–4529; i) C.-H. Jun, C. W. Moon, D.-Y. Lee, *Chem. Eur. J.* **2002**, *8*, 2423; j) C.-H. Jun, H. Lee, *J. Am. Chem. Soc.* **1999**, *121*, 880; k) C.-H. Jun, D.-Y. Lee, H. Lee, J.-B. Hong, *Angew. Chem. Int. Ed.* **2000**, *39*, 3070; l) C.-H. Jun, H. Lee, S.-G. Lim, *J. Am. Chem. Soc.* **2001**, *123*, 751; m) H. Salem, Y. Ben-David, L. J. W. Shimon, D. Milstein, *Organometallics* **2006**, *25*, 2292–2300.

[5] Gaussian 03, Revision B.01, M. J. Frisch, G. W. Trucks, H. B. Schlegel, G. E. Scuseria, M. A. Robb, J. R. Cheeseman, J. A. Montgomery Jr, T. Vreven, K. N. Kudin, J. C. Burant, J. M. Millam, S. S. Iyengar, J. Tomasi, V. Barone, B. Mennucci, M. Cossi, G. Scalmani, N. Rega, G. A. Petersson, H. Nakatsuji, M. Hada, M. Ehara, K. Toyota, R. Fukuda, J. Hasegawa, M. Ishida, T. Nakajima, Y. Honda, O. Kitao, H. Nakai, M. Klene, X. Li, J. E. Knox, H. P. Hratchian, J. B. Cross, C. Adamo, J. Jaramillo, R. Gomperts, R. E. Stratmann, O. Yazyev, A. J. Austin, R. Cammi, C. Pomelli, J. W. Ochterski, P. Y. Ayala, K. Morokuma, G. A. Voth, P. Salvador, J. J. Dannenberg, V. G. Zakrzewski, S. Dapprich, A. D. Daniels, M. C. Strain, O. Farkas, D. K. Malick, A. D. Rabuck, K. Raghavachari, J. B. Foresman, J. V. Ortiz, Q. Cui, A. G. Baboul, S. Clifford, J. Cioslowski, B. B. Stefanov, G. Liu, A. Liashenko, P. Piskorz, I. Komaromi, R. L. Martin, D. J. Fox, T. Keith, M. A. Al-Laham, C. Y. Peng, A. Nanayakkara, M. Challacombe, P. M. W. Gill, B. Johnson, W. Chen, M. W. Wong, C. Gonzalez, and J. A. Pople, Gaussian, Inc., Pittsburgh, PA, **2003**.

[6] a) C. A. Tolman, *Chem. Rev.* **1977**, *77*, 313; b) R. Mason, D. W. Merck, *Angew. Chem.* **1978**, *90*, 195; *Angew. Chem. Int. Ed. Engl.* **1978**, *17*, 183; c) P. S. Pregosin, *Transition Metal Nuclear Magnetic Resonance*, Elsevier Science Publishers **1991**, Amsterdam, The Netherlands; d) C. Brevard, P. Granger, *Handbook of High Resolution Multinuclear NMR*, John Wiley & Sons Inc., Chichester, UK, **1981**.

[7] a) J. G. Verkade, L. D. Quin, *Phosphorus-31 NMR Spectroscopy in Stereochemical Analysis*, VCH Publishers, Weinheim, Germany, **1987**; b) D. W. White, J. G. Verkade, *J. Magn. Reson.* **1970**, *3*, 111–116; c) M. Kainosho, A. Nakamura, *Tetrahedron* **1969**, *25*, 4071–4081.

[8] a) S. Otsuka, T. Yoshida, M. Matsumoto, K. Nakatsu, *J. Am. Chem. Soc.* **1976**, *98*, 5850–5858; b) A. C. Cooper, E. Clot, J. C. Huffman, W. E. Streib, F. Maseras, O. Eisenstein, K. G. Caulton, *J. Am. Chem. Soc.* **1999**, *121*, 97–106; c) G. Ujaque, A. C. Cooper, F. Maseras, O. Eisenstein, K. G. Caulton, *J. Am. Chem. Soc.* **1998**, *120*, 361–365; d) A. Cooper, W. E. Streib, O. Eisenstein, K. G. Caulton, *J. Am. Chem. Soc.* **1997**, *119*, 9069–9070; e) W. Baratta, E. Herdtweck, *Angew. Chem. Int. Ed.* **1999**, *38*, 1629–1631; f) R. L. Harlow, D. L. Thorn, R. T. Baker, N. L. Jones, *Inorg. Chem.* **1992**, *31*, 993–997; g) J. Fawcett, J. H. Holloway, G. C. Saunders, *Inorg. Chim. Acta* **1992**, *202*, 111–113; h) R. Cini, A. Cavaglioni, *Inorg. Chem.* **1999**, *38*, 3751–3754; i) D. Huang, W. E. Streib, J. C. Bollinger, K. G. Caulton, R. F. Winter, T. J. Scheiring, *J. Am. Chem. Soc.* **1999**, *121*, 8087–8097; j) R. H. Heyn, S. A. Macgregor, T. T. Nadasdi, M. Ogasawara, O. Eisenstein, K. G. Caulton, *Inorg. Chim. Acta* **1997**, *259*, 5–26; k) A. C. Albeñiz, G. Schulte, R. H. Crabtree, *Organometallics* **1992**, *11*, 242–249; l) M. Brookhart, M. L. H. Green, L.-L. Wong, *Prog. Inorg. Chem.* **1988**, *36*, 1–124.

[9] a) X.-L. Luo, R. H. Crabtree, *J. Am. Chem. Soc.* **1990**, *112*, 6912–6918; b) E. Gutierrez-Puebla, A. Monge, M. Paneque, M. L. Poveda, S. Taboada, M. Trujillo, E. Carmona, *J. Am. Chem. Soc.* **1999**, *121*, 346–354; c) W. J. Oldham, A. S. Hinkle, D. M. Heinekey, *J. Am. Chem. Soc.* **1997**, *119*, 11028–11036; d) M. Saunders, L. Telkowski, M. R. Kates, *J. Am. Chem. Soc.* **1977**, *99*, 8070–8071; e) R. B. Calvert, J. R. Shapley, *J. Am. Chem. Soc.* **1978**, *100*, 7726–7727; f) H.-U. Siehl, *Adv. Phys. Org. Chem.* **1987**, *23*, 63–165.

[10] J. Chatt, L. M. Vallarino, L. M. Venanzi, *J. Chem. Soc.* **1957**, 2496–2505; b) L. E. Crascall, J. L. Spencer, *Inorg. Synth.* **1990**, *28*, 126–135; c) P. J. Buss, B. Greene, M. Orchin, *Inorg. Synth.* **1990**, *20*, 181–182.

[11] a) A. L. van Geet, *Anal. Chem.* **1970**, *42*, 679–680; b) H. Friebolin, G. Schilling, L. Pohl, *Org. Magn. Reson.* **1979**, *12*, 569–573; c) C. Piccinni-Leopardii, O. Fabre, J. Reisse, *Org. Magn. Reson.* **1976**, *8*, 233–236; d) F. H. Köhler, X. Xie, *Magn. Reson. Chem.* **1997**, *35*, 487–492; e) J. Bornais, S. Brownstein, *J. Magn. Reson.* **1978**, *29*, 207–211.

[12] a) Data Collection Software for Nonius κ-CCD devices, Delft (The Netherlands), **2001**; b) Z. Otwinowski, W. Minor, *Methods Enzymol.* **1997**, *276*, 307; c) *SIR92*: A. Altomare, G. Cascarano, C. Giacovazzo, A. Guagliardi, M. C. Burla, G. Polidori, M. Camalli, *J. Appl. Crystallogr.* **1994**, *27*, 435–436; d) *International Tables for Crystallography*, Vol. C, Tables 6.1.1.4, 4.2.6.8, and 4.2.4.2 (Ed.: A. J. C. Wilson), Kluwer Academic Publishers, Dordrecht (The Netherlands), **1992**; e) A. L. Spek, PLATON, *A Multipurpose Crystallographic Tool*, Utrecht University, Utrecht, The Netherlands, **2001**; f) G. M. Sheldrick, *SHELXL-97*, University of Göttingen, Germany, **1998**.

Received: September 12, 2006
Published Online: January 23, 2007

